Journal of Materials Research and Technology 40 (2026) 1769–1793

Contents lists available at ScienceDirect

Journal of Materials Research and Technology

journal homepage: www.elsevier.com/locate/jmrt

Stretchable conductive Fibers: A quantitative and strategic review from materials to applications

Kangto Han [a,1], Eunho Lee [b,1], Jinsu Yun [a], Gyojic Shin [c], Chanmin Lee [c,d,*], Siyoung Lee [e,**], Geun Yeol Bae [a,***]

[a] Department of Materials Design Engineering, Kumoh National Institute of Technology, Gumi, 39177, South Korea
[b] Department of Chemical and Biomolecular Engineering, Seoul National University of Science and Technology, Seoul, 01811, South Korea
[c] Green Circulation R&D Department, Research Institute of Sustainable Development Technology, Korea Institute of Industrials Technology (KITECH), Cheonan, 31056, South Korea
[d] Department of Chemical Engineering, Chung-Ang University, Seoul, 06974, South Korea
[e] Advanced Bio and Healthcare Materials Research Division, Korea Institute of Materials Science (KIMS), Changwon, 51508, South Korea

ARTICLE INFO

Keywords:
Stretchable conductive fiber
Electronic textiles (E-textiles)
Stretchable structure
Conductive materials
Quantitative analysis

ABSTRACT

Stretchable conductive fibers (SCFs) are central to the advancement of electronic textiles (E-textiles), providing reliable electrical performance under large mechanical deformation. Conventional conductive fibers, often constrained by rigidity and mechanical failure, have been surpassed by SCFs that integrate structural engineering, advanced conductive materials, and scalable processing strategies. This review delivers a systematic overview of recent progress, addressing key performance parameters such as stretchability, elastic modulus, initial conductivity, and gauge factor. Particular emphasis is placed on structural designs and material strategies that tailor mechanical compliance and electrical stability, as well as fabrication methods that enable scalable implementation.

A distinguishing feature of this work is the quantitative evaluation of 124 studies reported over the past decade, establishing correlations between structural designs, conductive material dimensionalities, and combined electrical–mechanical properties. The analysis highlights how the choice of conductive material and structural geometry governs stretchability, conductivity, and strain response, offering generalizable insights that extend beyond individual case studies. In addition, remaining unresolved challenges, including wash durability, biocompatibility, chemical stability, and dyeability, all of which are indispensable for practical application, were discussed in depth. By consolidating qualitative trends with quantitative evidence, this review not only provides a comprehensive overview of the current state of SCF research but also outlines strategic directions for advancing their transition from laboratory prototypes to scalable and commercially viable E-textile systems.

1. Introduction

Deformable electronic devices that maintain their electrical functionality even under large deformations can naturally conform to human skin, offering significant potential for applications in diverse fields such as healthcare, military, sports, soft robotics, and virtual/augmented reality [1,2]. In particular, electronic textile (E-textile), a form of deformable electronics developed through recent advances in materials science and nanotechnology, is gaining attention as next-generation electronic devices, as they can be integrated into garments to improve human health and quality of life [3]. E-textiles go beyond the aesthetics, protection, and insulation functions that conventional textiles and garments have provided for thousands of years, demonstrating capabilities in sensing, energy harvesting, heating, and more [4,5].

Conductive fibers, typically characterized by a high aspect ratio (e.g., greater than 50), are essential for stable signal transmission and information exchange in E-textiles, and thus must exhibit sufficiently high electrical conductivity [6–8]. To date, such fibers have primary been

* Corresponding author. Research Institute of Sustainable Development Technology, Korea Institute of Industrials Technology (KITECH), South Korea.
** Corresponding author. Advanced Bio and Healthcare Materials Research Division, Korea Institute of Materials Science (KIMS), South Korea.
*** Corresponding author. Department of Materials Design Engineering, Kumoh National Institute of Technology, South Korea.
E-mail addresses: clee@kitech.re.kr (C. Lee), siyoungl@kims.re.kr (S. Lee), gybae@kumoh.ac.kr (G.Y. Bae).
[1] K. Han and E. Lee contributed equally to this work.

https://doi.org/10.1016/j.jmrt.2025.12.232
Received 30 October 2025; Received in revised form 16 December 2025; Accepted 22 December 2025
Available online 23 December 2025

fabricated by employing fine conductive metal wires and by incorporating or coating conductive materials onto conventional yarns [9]. However, the conductive fibers fabricated using rigid conductive materials often neglect the need for stretchability, making them prone to mechanical failure under deformation. This limits the electrical and mechanical durability of E-textiles and restricts their ability to conform to dynamic body movements during long-term wear, resulting in potential discomfort by skin pressure [10,11].

A promising alternative to conventional conductive fibers is the stretchable conductive fiber (SCF), which offers notable advantages such as high stretchability and stable electrical performance under mechanical strain. The term 'stretchable' is often interpreted similarly to 'elastic', as it implies not only the ability to elongate but also to recover to the original configuration [12]. This is a critical requirement in the field of E-textiles, where fibers must accommodate dynamic deformations induced by human motion. Over the past decade, research on SCFs has gained substantial momentum and now represents an expanding share of the overall E-textile research landscape (Fig. 1), underscoring their strong potential for future development [13].

This review aims to provide a comprehensive overview of research trends in SCFs, organized into materials and structural designs, fabrication methods, and emerging applications. Notably, to the best of our knowledge, this is the first study to provide a quantitative analysis of recent advances and distinctive characteristics in diverse research approaches to SCFs, based on 124 studies published over the past decade, with particular emphasis on both electrical and mechanical performance. Section 2 introduces the key performance metrics of SCFs, including stretchability, elastic modulus, initial conductivity, and gauge factor. Section 3 discusses strategies in structural design, material selection, and fabrication methods to enhance stretchability and optimize electrical performance. Section 4 highlights recent applications of SCFs in functional components such as stretchable bio-electrodes, sensors, heaters, displays, and energy harvesters. Section 5 presents a quantitative analysis of previous studies, and critically discusses the effects of structural designs, material dimensionality, and material types on SCF performance based on are graphical illustration. Finally, Section 6 outlines future research directions and technical challenges for the practical implementation of SCFs. This review is expected to serve as a comprehensive and structured reference for researchers in the fields of stretchable devices and E-textiles, while also providing clear directions to advance future research, practical implementation, and technological innovation.

2. Key properties of SCFs

To enable their practical use in E-textile subjected to diverse mechanical deformations, SCFs must ensure wearer comfort while maintaining both mechanical and electrical performance. Achieving this necessitates careful consideration of essential physical parameters, such as stretchability, elastic modulus, initial conductivity, and a gauge factor (GF). As these properties are interdependent, the materials, structural designs, and fabrication techniques should be comprehensively optimized to tailor the fibers for specific performance requirements [2].

2.1. Mechanical properties of SCFs

2.1.1. Stretchability

SCFs are required to possess substantial stretchability to accommodate the natural mechanical deformations associated with human body movements. Specifically, anatomical regions such as the wrist, knee, elbow, and shoulder undergo significant stretching and bending during typical motion. For example, the knee experiences a strain of approximately 43 %, the elbow around 44 %, the wrist about 22 %, and the shoulder approximately 38 % [14–16]. Since various body regions undergo substantial mechanical deformation, SCFs must be designed to accommodate the deformation required for different E-textile applications, including sportswear, rehabilitation garments, and military wearable systems. SCFs should also exhibit high cyclic stretchability, defined as the capability to retain their mechanical integrity and stable electrical performance under repeated stretching–release cycles ranging from thousands to hundreds of thousands. This characteristic serves as a critical indicator of the long-term reliability, durability, and commercial viability of stretchable conductive fibers in practical wearable systems.

2.1.2. Elastic modulus

The elastic modulus, which reflects the slope of the linear segment in a stress–strain curve, is a critical mechanical parameter indicating how much the fiber deforms under applied force. This property directly affects key performance metrics, including flexibility and stretchability, response and recovery times, as well as mechanical durability [11,17].

Fibers with a high elastic modulus tend to become rigid, which reduces durability and impairs wearer comfort by hindering natural body movements. When used as bio-electrodes, their high stiffness prevents conformal contact with the skin, making accurate bio-signal detection challenging. Similarly, when employed as sensors, their rigidity hinders precise signal detection under mechanical deformation. Recent studies suggest that, to ensure adequate mechanical conformity with the skin,

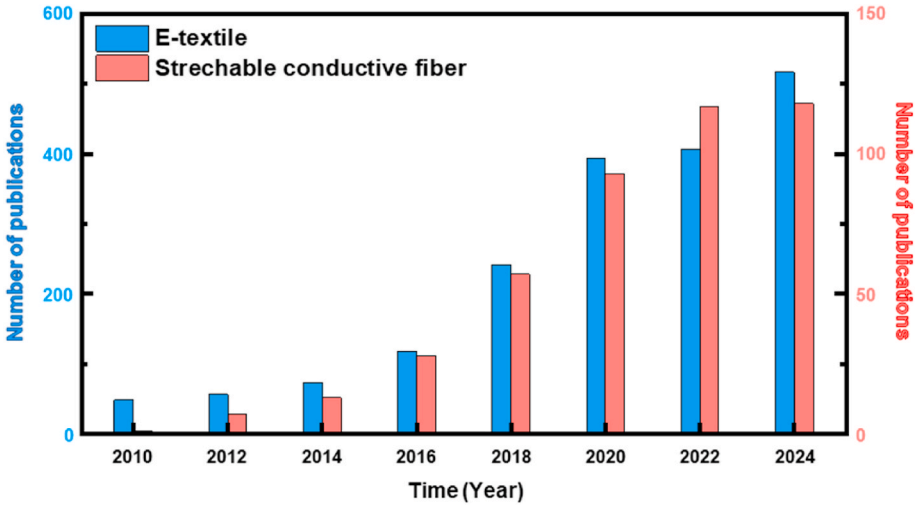

Fig. 1. The number of published research articles in each year about keywords of 'electronic textiles (E-textiles)' and 'stretchable conductive fiber' from 2010 to 2024. The data were obtained from the Web of Science by September 2025.

the elastic modulus of SCFs should be lower than that of human skin, which ranges approximately from 25 to 220 kPa [18]. To meet these requirements, conductive materials with intrinsically low elastic moduli, such as liquid metals, conductive hydrogels, conductive polymers, and ionic liquids, have been incorporated into SCFs [19–22]. However, SCFs with excessively low elastic modulus may exhibit prolonged response and recovery times, as well as hysteresis (i.e., energy loss during repetitive stretching and release cycles). Thus, selecting an optimal elastic modulus tailored to the intended application is critical for achieving desired functionality in SCFs [23].

2.2. Electrical properties of SCFs

2.2.1. Initial conductivity

The initial conductivity of SCFs is a critical parameter that defines their electrical properties in the absence of mechanical deformation. For SCFs to function reliably as interconnectors, electrodes, or wearable heaters in practical E-textile applications, their initial conductivity must remain high and stable [10,12,24,25]. Additionally, the fibers should be resistant to changes in initial conductivity that could arise from corrosion of the conductive materials due to exposure to sweat or water [26]. In contrast, when SCFs are used in physical sensors for monitoring pressure, strain, temperature, or humidity, high initial conductivity can negatively impact sensitivity by reducing the degree of resistance change [27,28].

The initial conductivity can be optimized through the careful selection of conductive materials, their dimensions, concentrations, and related parameters. This optimization is strongly governed by percolation theory, which explains that electrical resistance drops sharply once the volume fraction of conductive fillers exceeds a critical threshold. Beyond this point, the initial conductivity approaches saturation at a high level. However, an excessive incorporation of fillers, although maintaining high conductivity, undesirably increases the elastic modulus of the fiber [29]. Therefore, in designing SCFs, it is essential to judiciously determine both the type and concentration of conductive materials to achieve an optimal balance between electrical performance and mechanical properties [24].

2.2.2. Gauge factor

The gauge factor (GF) is the ratio of relative change in electrical resistance to the mechanical strain. This parameter is crucial for determining the appropriate application areas of SCFs. Fibers with a low GF are particularly suitable for wearable antennas, electrodes, and interconnectors, where stable electrical conductivity during deformation is essential. In contrast, fibers exhibiting a high GF can be employed as wearable sensors, where significant changes in resistance are required for effective sensing [30].

The GF of SCFs can be effectively tuned by adopting structural designs such as helical, serpentine, wrinkled, or porous forms, which relieve or amplify material strain through geometrical deformation [31–33]. Furthermore, selection of conductive material and controlling the percolation behavior is pivotal for modulating the GF of composite-based SCFs. In particular, conductive fillers with a relatively low concentration near the percolation threshold often results in significant resistance changes under mechanical deformation. In contrast, when the concentration exceeds the percolation threshold, stable quantum tunneling currents between numerous adjacent conductive domains enable the electrical resistance to remain relatively unchanged even under mechanical deformation [13].

3. Design and fabrication of SCFs

Conventionally, SCFs have been fabricated via two primary strategies: improving the stretchability of inherently conductive fibers or imparting electrical conductivity to intrinsically stretchable fibers. In the first approach, stretchability is improved by introducing geometrically engineered structures. In the second approach, intrinsically stretchable polymeric materials are rendered conductive by incorporating conductive fillers, such as carbon-based materials, metal-based materials, MXene, liquid metals, conductive polymers, or ionic liquids [34,35]. Recently, to enhance the mechanical and electrical stretchability of SCFs, diverse combinations of structures and materials have been adopted, and they have been fabricated using various techniques, including spinning, coating, and physical or chemical deposition processes [36].

3.1. Structural design

Structural design refers to a strategy in which mechanically engineered structures, such as helical, serpentine, wrinkled, and porous structures, are introduced into fibers to enhance their stretchability. These structures serve to reduce the effective modulus of SCFs and enable high fracture strain by minimizing the direct elongation of the fibers under external deformation. Among these structures, helical, serpentine, and wrinkled forms effectively suppress the change in electrical resistance, thereby leading to a lower GF [37]. In contrast, SCFs with porous structures often exhibit greater resistance changes during stretching, resulting in higher GFs, due to the elongated current paths created by pore expansion [16].

3.1.1. Helical structure

Helical structure enables high stretchability without exceeding the material's mechanical limits, as fiber length can be increased through changes in helical curvature rather than through direct elongation under external force. This behavior is depicted in Fig. 2a and can be described by Equation (1) [38].

$$S^2 = L^2 + (\pi ND)^2 \tag{1}$$

When the helical structure is laid flat horizontally, it shows a right-angled triangle relation with the following parameters. The hypotenuse length, S, represents the actual length of the helix; L denotes the vertical fiber length; N indicates the total number of helical turns; and D represents the helix diameter. The maximum strain (ε) of the helix, derived using Equation (1), is presented in Equation (2), which indicates that ε increases with higher N and larger D.

$$\varepsilon = \frac{S - L}{L} = \frac{\sqrt{L^2 + (\pi ND)^2} - L}{L} \tag{2}$$

Morikawa et al. developed a hydrogel-based SCF featuring a helical structure and showed that increasing N and D improves stretchability [39]. The SCF with a straight form, lacking a helical structure, exhibited limited stretchability with a fracture strain of only 35 % and a relatively high GF of approximately 45.71 within the 0–35 % strain range. In sharp contrast, the SCF with a helical structure demonstrated remarkable extensibility, reaching a fracture strain of 800 %, a much lower GF of 0.017 over the 0–600 % strain range, and an initial conductivity of 16.8 S/m. In a similar study, Shang et al. prepared a polyurethane (PU)/carbon nanotube (CNT)/MXene-based SCF with a helical configuration using external tension. They observed that as the external tension decreased (from 11.49 MPa to 3.86 MPa), D increased (from 52.8 μm to 55.7 μm), which consequently enhanced stretchability from 370 % to over 800 %. The SCF achieved an initial conductivity of 1.5×10^5 S/m and maintained a low GF of 1.06 at 200 % strain [40]. (Fig. 2b) In addition, Yu et al. fabricated a helical-structured SCF by twisting and coiling thermoplastic polyurethane (TPU) fibers coated with silver nanoparticles (AgNPs) [41]. (Fig. 2c) The conductive fiber without a helical design, as a reference, exhibited a stretchability of only approximately 175 % and high GF of 31.9 under 80 % strain. In contrast, introducing the helical structure increased the stretchability of 300 % and achieved a low GF of approximately 1 under 80 % strain.

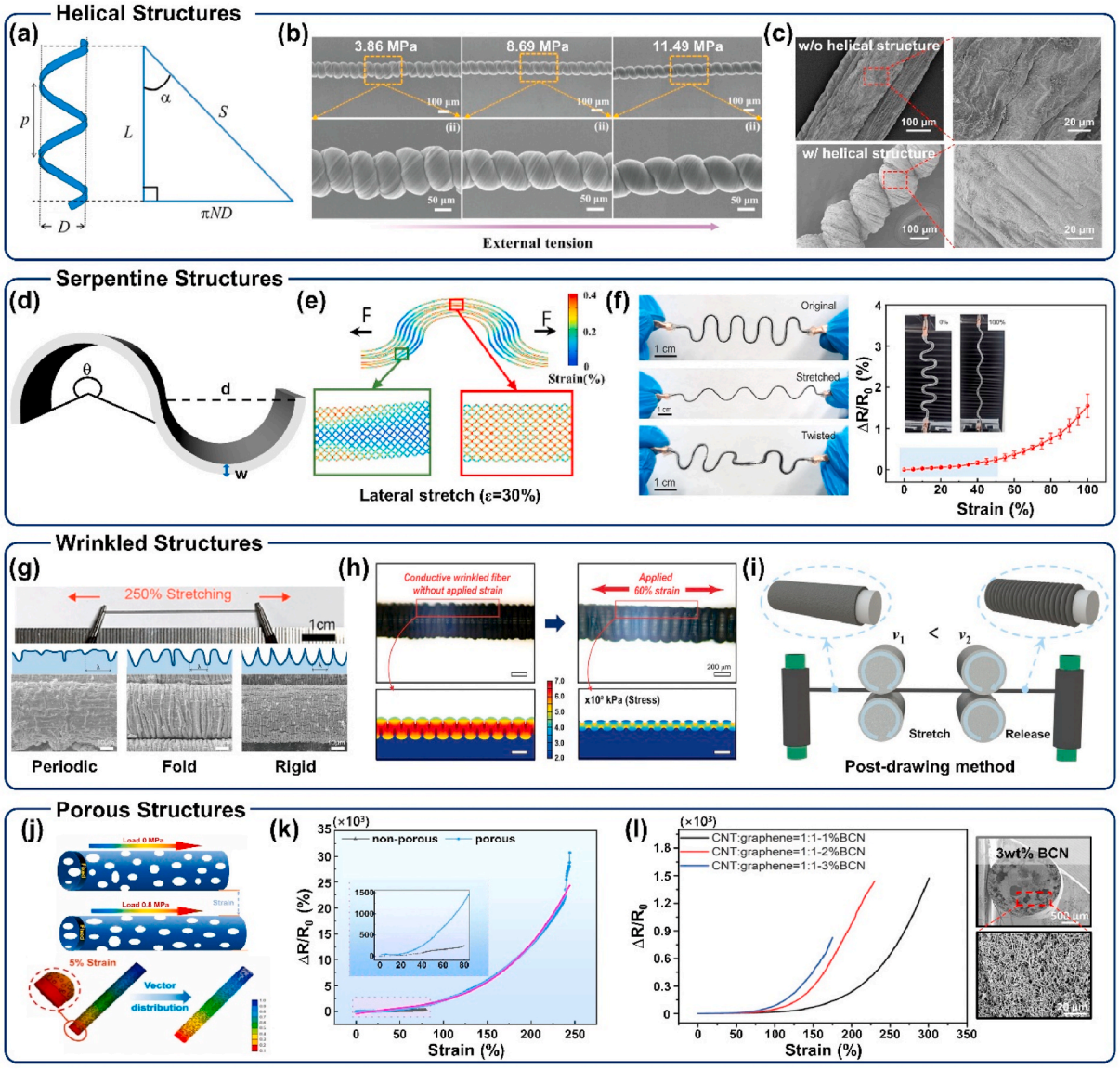

Fig. 2. Representative structures of stretchable conductive fibers (SCFs): a-c) Helical structures; d-f) Serpentine structures; g-i) Wrinkled structures; j-l) Porous structures. a) Geometry of the helix illustrated as an opened-up right-angle triangle. The parameters are explained in Eq. (1). Reproduced with permission from ref 38. Copyright 2019 Wiley. b) SEM images of helical structured SCFs under different external tension. Reproduced with permission from ref 40. Copyright 2023 Wiley. c) SEM images of the SCFs with and without a helical structure. Reproduced with permission from ref 41. Copyright 2023 Wiley. d) Schematics of serpentine structural parameters. The parameters are explained in Eqs. (3) and (4). e) FEM analysis result of stretch deformations and strain distribution of the SCF along transverse directions. Reproduced with permission from ref 43. Copyright 2020 Elsevier. f) Photographs illustrating the stretchability of serpentine structured SCFs and relative resistance change ($\Delta R/R_0$) as a function of applied strain. Reproduced with permission from ref 1. Copyright 2023 Elsevier. g) SEM images of the SCFs with and without a wrinkled structure. Reproduced with permission from ref 46. Copyright 2023 ACS. h) Optical microscope images and FEM results of the micro-wrinkled SCF with and without an external strain (60 %). Reproduced with permission from ref 45. Copyright 2020 Wiley. i) Schematic illustration of wrinkled SCFs fabricated via the post-drawing method. Reproduced with permission from ref 47. Copyright 2023 Elsevier. j) Tensile behavior of porous fiber. Reproduced with permission from ref 49. Copyright 2024 Elsevier. k) Relative resistance change ($\Delta R/R_0$) of non-porous and porous structured SCFs under strain. Reproduced with permission from ref 52. Copyright 2022 Elsevier. l) Relative resistance change ($\Delta R/R_0$) of SCFs with different Bacterial Cellulose Nanofiber (BCN) cont. and SEM image of SCFs with 3 wt% BCN. Reproduced with permission from ref 53. Copyright 2021 Wiley.

3.1.2. *Serpentine structure*

Unlike helical-structured SCFs, serpentine-structured SCFs can be implemented in a two-dimensional plane. Lu et al. derive the maximum strain (ε) for the serpentine configuration, as expressed in Equations (3) and (4) and illustrated in Fig. 2d [42].

$$\varepsilon = \frac{\theta}{2\sin\left(\frac{\theta}{2}\right)} \tag{3}$$

$$\varepsilon \propto \frac{d}{w} \tag{4}$$

In this equation, θ represents the central angle, w denotes the width of fiber, and d refer to diameter of curved beams. This relationship indicates that ε of the serpentine structure increases as w decrease, while increasing $\theta$and d. Song et al. fabricated a serpentine-structured stretchable conductive sheet based on silver (Ag) nanofibers via electrospinning and metal deposition (Fig. 2e) [43]. The fabricated sheet achieved a sheet resistance of 9.0 Ω/sq. While the sheet with w of 500

μm exhibited a high GF of 7.69 under a low stretchability of 26 %, reducing the width to 25 μm enabled the sheet to withstand 50 % strain while maintaining a low GF of less than 0.2. Similarly, Wang et al. developed a serpentine SCF composed of multi-walled carbon nanotubes (MWCNT) and waterborne polyurethane (WPU) using a molding process. (Fig. 2f) [1]. Without the serpentine configuration, the fiber exhibited a fracture strain of approximately 17 %. In contrast, with the incorporation of the serpentine structure, the SCF withstood 100 % strain without mechanical failure, exhibiting an initial conductivity of 1552 S/m and maintaining a GF of 1.6 under 0–100 % strain range.

3.1.3. Wrinkled structure

Wrinkled structures in multilayered conductive fibers are formed upon the release of pre-strain, resulting from differences in elastic moduli between stiff conductive layers and soft polymer substrates [44]. At this point, the ratio between the unit lengths with and without micro wrinkles (r_w) is defined by Equation (4) [45].

$$r_w \sim \frac{\pi}{8} + 2\left(\sqrt{\varepsilon - \varepsilon_c}\right) \tag{4}$$

The ε represents applied pre-strain, and ε_c denotes critical strain. According to Equation (4), A higher pre-strain generates wrinkles with larger r_w, which in turn contributes to enhancing the stretchability of the fiber. Lee et al. fabricated wrinkled SCFs based on AgNPs and PU (Fig. 2g) [46]. By adjusting the pre-strain level and controlling the formation of AgNPs, they tuned both the wavelength and morphology of the wrinkled structures. As the pre-strain increased or a greater amount of AgNPs was introduced onto the fiber surface, the elastic modulus mismatch between the PU matrix and the AgNPs layer became more pronounced, resulting in the formation of wrinkles with shorter wavelengths. This, in turn, led to significant reduction in GF. Without the wrinkled structure, the conductive fiber exhibited an extremely high GF of 18100 under 200 % strain. However, the introduction of the wrinkled structure markedly reduced the GF value to 1.8 under the same strain. Pang et al. fabricated a SCF featuring a wrinkled structure by pre-straining spandex fibers, coating them with a Poly(3, 4-ethylenedioxythio-phene):poly(styrenesulfonate) (PEDOT:PSS)/single-walled carbon nanotube (SWCNT)/PU composite, and subsequently releasing the strain to induce the wrinkled morphology (Fig. 2h) [45]. The fabricated SCF exhibited an initial conductivity lower than 10^4 S/m. Without the wrinkled structure, the fiber showed GF of 15 under approximately 0–40 % strain range. In contrast, incorporating the wrinkled structure reduced the GF of 0.033 under 60 % strain. Similarly, Mao et al. developed a SCF based on a PU/polypyrrole (PPy) composite, controlling the wavelength of the wrinkled structure via continuous post-drawing methods (Fig. 2i) [47]. The fabricated SCF could withstand strains up to 850 % without fracture, achieved an initial conductivity of 529 S/m, and achieved a low GF of 0.07 under 50 % strain. Moreover, it was demonstrated that decreasing the wavelength of wrinkles led to a reduction in the elastic modulus of the SCF.

3.1.4. Porous structure

Porous structure refers to a configuration in which pores are introduced within the SCF [48]. For fibers with porous architectures, the effective stress carried by the bulk region is substantially reduced relative to dense fibers, since the porous domains inside the fiber accommodate most of the strain. These pores act as strain-buffering domains, which not only enhance the overall flexibility of the fiber but also decrease its effective modulus. (Fig. 2j) [49]. Furthermore, as the pores inside the fiber accommodate much of the effective stress, they tend to expand and generate microcracks under tensile strain, thereby producing a larger resistance change during stretching [16,50].

Yuan et al. fabricated a porous SCF using MXene and PU via wet spinning [51]. The fabricated fiber showed an initial conductivity of less than 1 S/m at 5 wt % MXene content. Without pores, the fiber exhibited a fracture strain of 874 %, while the presence of the pores increased the fracture strain to 1016 %. Notably, under 50 % strain, the porous fiber exhibited a GF of 820, more than twice the value measured in non-porous fibers. Similarly, Yin et al. produced porous SCF by spray-coating CNT/Styrene-Ethylene-Butylene-Styrene (SEBS) ink onto PU fibers (Fig. 2k). The non-porous fiber demonstrated a GF of approximately 3.13 at 80 % strain, whereas the porous one exhibited a significant GF of 18.75 at same strain [52]. Wang et al. prepared a TPU/CNT/Graphene/bacterial cellulose nanofibers (BCN)-based SCF with a porous structure using wet spinning. With the addition of hydrophilic BCN, the speed of double diffusion slowed down, leading to smaller pore sizes and increased porosity. When 1 wt% BCN was incorporated, the SCF exhibited a stretchability of 150 % and a GF of 16.1 at 100 % strain, whereas with 3 wt% BCN, the stretchability increased to 300 % and the GF reached 193.3 at around 100 % strain [53]. (Fig. 2l)

3.2. Material design

The type of conductive materials plays a critical role in determining both mechanical and electrical performance. The conductive materials currently employed in SCFs can be broadly categorized into carbon-based materials, metal-based materials, MXene, liquid metals, conductive polymers and ionic liquids.

Carbon-based and metal-based conductive materials offer high electrical conductivity, enabling excellent conductive pathways within SCFs. However, their use can often result in a trade-off between electrical and mechanical properties, which must be carefully managed by considering the form and intrinsic characteristics of the conductive materials [54]. Carbon-based and metal-based conductive fillers can be classified by their dimensionality into zero-dimensional (e.g., carbon black, metal nanoparticles), one-dimensional (e.g., carbon nanotubes, metal nanowires), and two-dimensional (e.g., graphene, MXene, metal nanoflakes) materials.

In addition to these conventional fillers, various alternative conductive materials have also been investigated to meet the demands for flexibility, stretchability, and biocompatibility in SCFs. Conductive polymers and ionic liquids, for example, offer inherent advantages such as high stretchability, self-healing capabilities, and biocompatibility [55,56]. Furthermore, liquid metals have emerged as promising candidates due to their excellent electrical conductivity and high deformability, which originates from their low melting point close to or below room temperature [57].

3.2.1. Carbon-based SCFs

Carbon-based conductive materials have been considered one of the most representative conductive components for incorporation into SCFs, owing to their multiple advantages such as high electrical conductivity (10^3–10^6 S/m), mechanical strength, wear and corrosion resistance, and overall stability [58]. Such materials include carbon black, carbon nanotubes (CNTs), and graphene, all of which enable free electron movement through their conjugated π-electron networks formed by sp^2 orbital hybridization [59]. SCFs, incorporating these materials, are typically manufactured either by coating carbon materials onto polymer substrates or by spinning fibers from composite solutions containing stretchable polymers and carbon-based fillers. In these processes, the uniform dispersion of the conductive fillers is crucial for achieving high electrical conductivity and uniform performance. However, carbon-based materials tend to aggregate easily due to strong π–π interactions, which presents a substantial challenge [60]. Accordingly, most research has aimed to improve the dispersibility of carbon-based nanomaterials in order to achieve outstanding electrical properties of SCFs [61]. For instance, Zhu et al. developed a SEBS/CNT-based SCF through wet spinning (Fig. 3a). The strong π–π interaction between the styrene blocks of SEBS and the CNTs, together with good interfacial compatibility, facilitated a uniform dispersion. This process yielded the SCF capable of withstanding 1140 % strain and exhibiting an initial

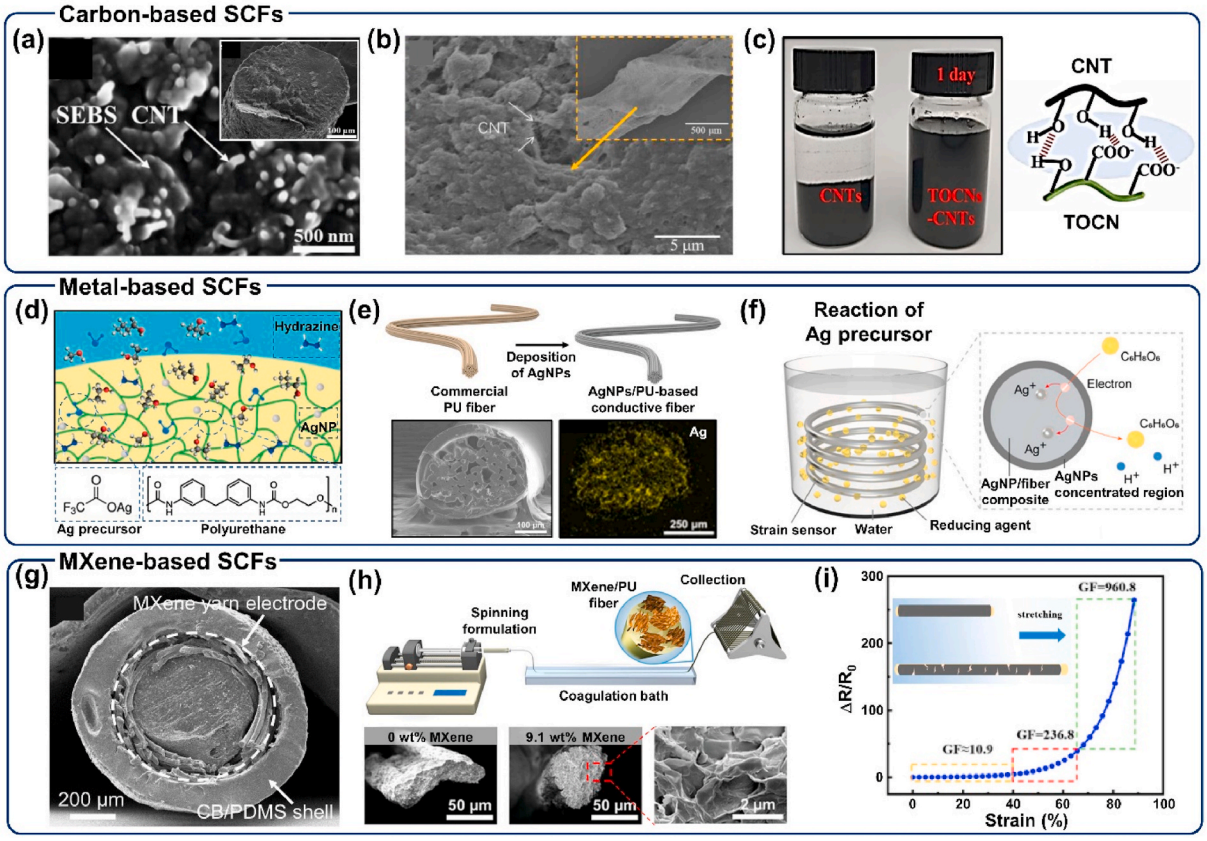

Fig. 3. Representative conductive materials used in SCFs: a-c) Carbon-based; d-f) Metal-based; g-i) MXene-based conductive materials; a) SEM image of uniformly dispersed CNT in SCF. Reproduced with permission from ref 62. Copyright 2021 Elsevier. b) SEM image of the surface of the CNT/double-threaded yarn (DTY) layer. Reproduced with permission from ref 63. Copyright 2024 Elsevier. c) Photographs of CNTs and TOCNs-CNTs formed in a dispersed state in water after 1 day, and mechanisms of interaction between components. Reproduced with permission from ref 64. Copyright 2024 Elsevier. d) Schematic illustrations of hydrazine reduction of the Ag precursor to obtain SCFs. Reproduced with permission from ref 69. Copyright 2020 Wiley. e) Schematic illustration of the fabrication process and SEM/EDS images of Ag-based SCFs. Reproduced with permission from ref 70. Copyright 2023 Wiley. f) Schematic illustration of Ag^+ reduction mechanism of the SCFs by L-ascorbic acid. Reproduced with permission from ref 71. Copyright 2021 ACS. g) SEM images of the cross-section of the MXene-based SCFs. Reproduced with permission from ref 75. Copyright 2024 Elsevier. h) Schematic of fabrication process for MXene-based SCFs and SEM images showing the morphology of SCF with and without MXene. Reproduced with permission from ref 76. Copyright 2020 Wiley. i) Relative resistance change ($\Delta R/R_0$) of MXene/WPU composite-coated SCFs under tensile strain. Reproduced with permission from ref 77. CC BY 4.0.

conductivity of 18.6 S/m and a GF of 368 under 471 % strain [62]. Likewise, Yan et al. produced a SCF by dip-coating CNTs onto double-threaded yarn (DTY) [63]. (Fig. 3b) Polyvinyl pyrrolidone (PVP) was added into the aqueous CNT dispersion as a binder and dispersant, which not only improved the dispersion of CNTs in water but also promoted hydrogen bonding between CNTs and DTY. The resulting fiber exhibited a fracture strain of around 150 %, and a GF of 12.4 even under 100 % strain. Similarly, Han et al. fabricated a CNT-based conductive hydrogel stretchable fiber via wet spinning (Fig. 3c) [64]. They introduced 2,2,6,6-Tetramethylpiperidine-1-oxyl (TEMPO)-oxidized cellulose nanofibers (TOCN) into the oxidized CNT dispersion, enhancing the stable dispersity of CNT dispersion utilizing hydrogen bonding. As a result, the fiber demonstrated high stretchability of 438 %, an initial conductivity of 1.57 S/m, and a GF of 1.47 within a strain range up to 50 %

3.2.2. *Metal-based SCFs*

Metal-based conductive materials, including aluminum (Al), copper (Cu), gold (Au), and silver (Ag), offer significant advantages such as high mechanical strength, excellent thermal conductivity, and electrical conductivity of approximately 5×10^7 S/m, attributed to their well-ordered lattice structures [65,66]. These attributes have fueled extensive research into developing SCFs by integrating metal-based conductive materials with stretchable polymer matrices. For example, Wang et al. developed a stretchable conductive non-woven fabric by electrospinning Ag NW-embedded PU nanofibers. The fabricated fabric displayed a remarkable stretchability of 800 %, and a GF of 55 under 0–40 % strain [67].

Notably, SCFs with metallic materials can also be fabricated by post-reduction of metal precursors. This method not only obviates the need for metal particle dispersion but also allows stable embedding of metal nanoparticles on or within the fiber, thereby enhancing uniformity and ensuring mechanical and electrical stability of the SCF [68]. Lee et al. fabricated AgNPs-embedded SCF by sequentially immersing Spandex fibers in Ag precursor solution, followed by treatment with hydrazine hydrate (N_2H_4) solution (Fig. 3d). The resulting fiber withstood strains up to 6812 % and exhibited a GF of 600 at 150 % strain, and initial conductivity to 3.05×10^6 S/m [69]. Additionally, Kim et al. fabricated a SCF based on AgNPs and PU via dip coating and subsequent reduction process of Ag precursor (1:1 vol mixture of hydrazine hydrate and ethanol) (Fig. 3e). The fabricated fiber achieved a stretchability of 100 % and a GF of 181 under 100 % strain [70]. In a similar effort, Lee et al. developed a SCF by dip-coating a stretchable fiber matrix with an Ag precursor, followed by chemical reduction using L-ascorbic acid. (Fig. 3f) [71]. They demonstrated that the fiber's electrical resistance decreased as the degree of Ag formation increased. The fabricated fiber matrix exhibited a GF of 91 at 0–50 % strain range and achieved a high initial conductivity of approximately 1×10^5 S/m.

3.2.3. MXene-based SCFs

MXene is a class of 2D nanomaterials characterized by outstanding electrical conductivity, ease of processing, and mechanical flexibility, which have found extensive applications across various technological fields since their discovery in 2011. They are synthesized by selectively removing the A layers from MAX phases, where M denotes an early transition metal, A corresponds to a group 13 or 14 element, and X represents carbon or nitrogen [72]. The etching of A-group elements from MAX phases typically involves the use of reagents such as hydrofluoric acid (HF), ammonium fluoride (NH_4F), sodium fluoride (NaF), calcium fluoride (CaF_2), or combinations such as hydrochloric acid (HCl) mixed with lithium fluoride (LiF) [73]. Through the etching process, the surfaces of the M layers become terminated with functional groups such as –OH, –O, and –F. The resulting MXene compounds are generally expressed as $M_{n+1}X_nT_x$, where T_x denotes surface terminations that enhance the materials' dispersibility in aqueous and, in certain cases, organic solvents, depending on their surface chemistry [74]. Jiang et al. engineered a core–shell structured SCF by applying a coating of carbon black (CB) and polydimethylsiloxane (PDMS) onto MXene-based fibers (Fig. 3g) [75]. The fabricated fiber exhibited a high fracture strain exceeding 250 %, an initial resistance of 0.25 kΩ/cm, and a GF of 0.124 under 100 % strain. Similarly, Gogotsi et al. developed a SCF using MXene/PU composite fibers manufactured via wet spinning (Fig. 3h). During the fabrication of SCFs, more circular fibers were obtained as the MXene content increased. This was because the high dispersibility of MXene facilitated the inward diffusion of polar solvents into the fiber. The resulting fiber showed a stretchability of up to 250 % and a GF of 238 under 50 % strain [76]. In another study, Wang et al. fabricated a SCF by dip-coating PU fibers with an MXene/WPU solution (Fig. 3i) [77]. In the solution, both MXene and WPU carried negative charges, inducing electrostatic repulsion that facilitates the uniform dispersion of MXene within the WPU matrix. The resulting fiber achieved a GF of 10.9 within a strain range of 0–40 %.

3.2.4. Liquid metal-based SCFs

Liquid metals such as mercury (Hg) and gallium (Ga) remain in a liquid state below 40 °C. Among them, gallium-based liquid metals have garnered significant interest as promising conductive materials for SCFs due to their high electrical conductivity, excellent deformability, and substantially lower toxicity compared to mercury [78]. However,

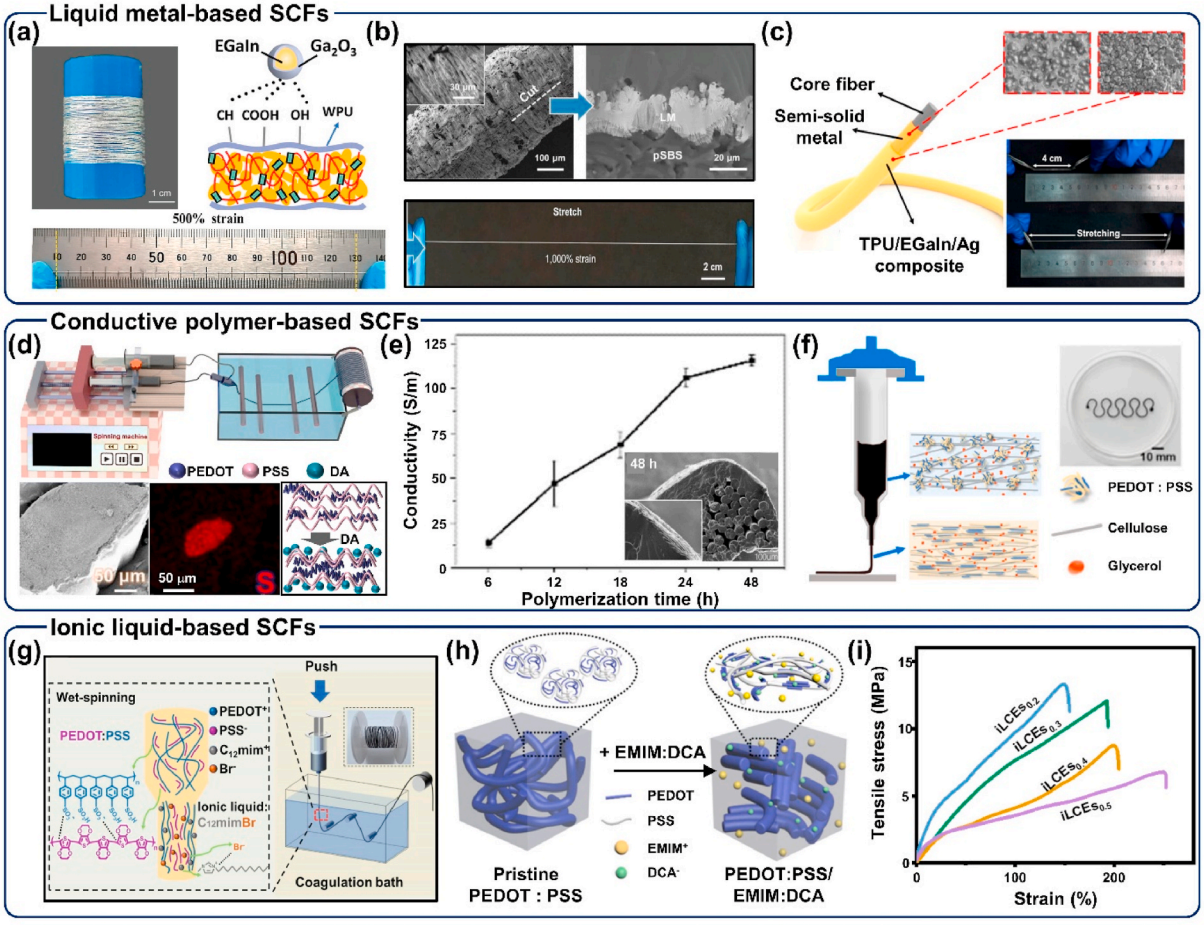

Fig. 4. Representative conductive materials used in SCFs: a-c) Liquid metals; d-f) Conductive polymers; g-i) Ionic liquids. a) Photographs of liquid metal-coated SCFs and schematic illustration of bonding mechanism induced by the Ga_2O_3 layer. Reproduced with permission from ref 82. Copyright 2023 Wiley. b) SEM image of liquid metal-coated stretchable conductive non-woven fabric exhibiting high interfacial compatibility with the SBS fibers. Reproduced with permission from ref 83. Copyright 2023 Wiley. c) Structural diagram of the SCF, consisting of core fiber, semisolid metal conducting layer, and TPU/EGaIn/Ag composite conducting layer and Optical images of the SCF before and after stretch. Reproduced with permission from ref 84. Copyright 2024 ACS. d) Fabrication schematic, SEM/EDS images, and dopamine-induced conductive mechanism of PEDOT:PSS based SCFs. Reproduced with permission from ref 87. Copyright 2025 Elsevier. e) Conductivity variation curves of PPy-based SCFs with different polymerization times and SEM image of SCF polymerized at 48 h. Reproduced with permission from ref 88. Copyright 2022 ACS. f) Schematic illustration of the components of the conducting ink and the printing process. Reproduced with permission from ref 89. CC BY 4.0. g) Schematic of fabrication for ionic liquid-based SCFs. Reproduced with permission from ref 92. Copyright 2023 Elsevier. h) Molecular structure of pristine PEDOT:PSS and PEDOT:PSS/EMIM:DCA. Reproduced with permission from ref 93. Copyright 2023 ACS. i) Tensile stress-strain curves as a function of the molar content of ionic liquid. Reproduced with permission from ref 95. Copyright 2024 Elsevier.

gallium-based liquid metals are prone to rapid oxidation even under low oxygen concentrations (>1 ppm), forming a Ga_2O_3 oxide layer ranging from 0.5 to 5 nm in thickness [79]. This oxide layer exhibits high surface tension (approximately 624 mN/m) and low electrical conductivity (around 22 S/m), which can negatively influence adhesion, wettability with polymer substrates, and the overall conductivity of SCFs [80,81]. Therefore, recent studies have focused on overcoming these drawbacks by enhancing the interfacial interactions between liquid metals and polymer materials. Xiong et al. fabricated a SCF by producing Ag flake/TPU fibers via wet spinning, followed by sequential coatings of WPU and eutectic Gallium–Indium (EGaIn), a gallium-based liquid metal with a melting point of approximately 16 °C (Fig. 4a) [82]. WPU facilitated hydrogen bonding between the oxygen atoms in Ga_2O_3 and functional groups such as –OH, –CH, and –COOH, enhancing adhesion between the liquid metal and the TPU substrate. The resulting SCF achieved a high fracture strain of 611 % and an initial conductivity of 3.13×10^5 S/m, as well as a GF of 0.5 within a strain range of 0–20 %. Zheng et al. developed a stretchable conductive non-woven fabric by electrospinning a poly(styrene-block-butadiene-block-styrene) (SBS) matrix, which was subsequently dip-coated with polyacrylic acid and Galinstan, a gallium-based liquid metal alloy consisting of gallium, indium, and tin (Fig. 4b) [83]. In this system, the carboxyl groups (–COOH) in polyacrylic acid induced hydrogen bonding between the oxide layer of Galinstan and the SBS substrate. The fabricated conductive fabric showed remarkable stretchability of approximately 1700 %, an initial conductivity of 6.9×10^3 S/m, and only a low GF of 0.6 under 0–1500 % strain range.

Moreover, the formation of intermetallic compounds can serve as an effective strategy to enhance the wettability between gallium-based liquid metal and polymer matrices. Wang et al. produced a SCF by dip-coating TPU fibers with an EGaIn/Ag mixture (Fig. 4c) [84]. The intermetallic phases formed between EGaIn and Ag facilitated enhanced metallic wetting, thus improving the interfacial compatibility between EGaIn and the TPU matrix. The fabricated fiber exhibited excellent stretchability of 600 %, an initial conductivity of 2.3×10^5 S/m, and a GF of 7.5 at 600 % strain.

3.2.5. Conductive polymer-based SCFs

Conductive polymers represent a class of organic functional materials that integrate the electrical characteristics of metals or semiconductors into conventional polymer systems. These materials feature conjugated molecular chains that enable charge transport, leading to inherent electrical conductivity. Well-known examples include polyacetylene, polythiophene, polyphenylene, poly(*p*-phenylene vinylene), poly(*p*-phenylene sulfide), and PEDOT:PSS [60,85]. These polymers offer significant advantages such as biocompatibility, low density, and cost-effectiveness, and can be blended into polymer matrices without severely compromising mechanical performance, making them promising candidates for SCF development [86].

However, conductive polymers generally exhibit lower electrical conductivity compared to carbon- or metal-based conductive materials, which poses a challenge for their application in high-performance stretchable electronics. Consequently, various strategies are under investigation to enhance the conductivity of SCFs based on conductive polymers. For example, Gao et al. fabricated a SCF by wet spinning a composite of PEDOT:PSS, sodium alginate, and polyvinyl alcohol (PVA) (Fig. 4d) [87]. When dopamine hydrochloride was incorporated during fiber fabrication, the initial conductivity increased from 539.3 S/m to 669.8 S/m. This improvement is attributed to the fact that dopamine can react with PSS groups to form a semi-quinone structure, thereby making the PEDOT:PSS stacks more regular. The resulting fiber showed a stretchability of 50 % and a GF of 0.8 % under 10 % strain. Also, Mao et al. developed a SCF by coating of PPy onto WPU/PU composite fibers [88]. (Fig. 4e) During the PPy coating process, cyclohexane solvent was used to facilitate interfacial polymerization, and as the polymerization time increased from 6 h to 48 h, the initial conductivity increased from 12.5 S/m to approximately 112.5 S/m. The fabricated fiber exhibited a fracture strain of approximately 1500 % and a GF of 0.11 within a strain range of 0–600 %. Similarly, Wagberg et al. used 3D printing to produce a SCF composed of PEDOT:PSS, dialcohol cellulose, and glycerol (Fig. 4f) [89]. The fabricated fiber displayed a fracture strain of around 50 % and a GF of 5 at 40 % strain. The study also demonstrated that increasing glycerol content from 1 vol % to 5 vol % raised the SCF conductivity from 2000 S/m to 3500 S/m, owing to dipole–dipole interactions between glycerol and the thiophene rings in PEDOT.

3.2.6. Ionic liquid-based SCFs

Ionic liquids are salts consisting of cations and anions that remain in a liquid state at temperatures generally below 100 °C [90]. Unlike traditional carbon- or metal-based conductive fillers, ionic liquids exhibit exceptionally low Young's moduli (<1 Pa), enabling SCFs with low stiffness. Additionally, the mechanical and electrical properties of such fibers can be adjusted by selecting different cation-anion combinations within the ionic liquid, providing significant deformability [91]. Gao et al. developed a SCF comprising PEDOT:PSS and an ionic liquid (1-dodecyl-3-methylimidazole bromide) via wet spinning (Fig. 4g) [92]. The fiber demonstrated a stretchability with a fracture strain of 60 % and achieved an initial conductivity of 1.2×10^4 S/m. Furthermore, it displayed temperature-dependent resistance changes, attributed to the temperature-induced variations in the ion mobility, which directly influence electrical conductivity. In a similar study, Wang et al. fabricated a SCF using PEDOT:PSS and an ionic liquid (1-Ethyl-3--methylimidazolium dicyanamide), also employing wet spinning (Fig. 4h) [93]. The resulting fiber exhibited a fracture strain of 27.7 %. The inclusion of the ionic liquid significantly enhanced the electrical conductivity from 1.5×10^5 to 4.3×10^5 S/m. This improvement was attributed to an ion-exchange reaction between the ionic liquid and PEDOT:PSS, which promoted the formation of a linear conformation. Qiao et al. fabricated a SCF by coating silk fibers with an ionic liquid (1-butyl-3-methylimidazole hexafluorophosphate) and poly(vinylidene fluoride-co-hexafluoropropylene) (PVDF-HFP) [94]. The introduction of the ionic liquid enhanced the fracture strain, and the resulting fiber exhibited an initial conductivity of 0.22 S/m together with a GF of 1.67 within the strain range of 0–15 %. Similarly, Li et al. fabricated an ionogel-based SCF by curing an ionic mixture within polytetrafluoroethylene (PTFE) tubes (Fig. 4i) [95]. As the ionic liquid content in the fiber increased from 20 mol % to 50 mol %, the fracture strain rose from approximately 150 % to around 250 %. The fabricated fiber achieved an initial conductivity of 2.3 S/m and maintained a GF of 0.51 within a strain range of 0–50 %.

3.3. Fabrication methods

SCFs have been fabricated using various methods, including spinning, coating, and chemical or physical vapor deposition (CVD or PVD). Spinning involves extruding a mixture of conductive materials and polymer matrices through spinnerets to produce intrinsically conductive and stretchable fibers, in which the conductive components are dispersed within the polymer matrix. In contrast, coating, CVD, and PVD techniques impart electrical conductivity by depositing thin conductive films onto deformable polymer-based fibers.

These geometrical features induced by the fabrication method significantly influence the failure behavior of SCFs under large elastic deformation, cyclic mechanical loading, and environmental stresses. First, SCFs based on composite fabricated via spinning often experience filler segregation and conductive-network rearrangement under high strain, generating filler-rich and -depleted regions, voids, and anisotropic percolation pathways [69,96]. These heterogeneities locally concentrate mechanical and electrical stresses, thereby promoting disconnections of electrical pathways. Second, SCFs fabricated via coating or deposition methods are more susceptible to fatigue-induced microcracking, as cyclic tensile or bending deformation localizes stress at stiff

conductor–soft matrix interfaces and within heterogeneous conductive networks [97]. This promotes progressive crack nucleation and propagation, ultimately severing conductive pathways and resulting in gradual resistance drift or abrupt open-circuit failures. In particular, surface-coated SCFs frequently undergo interfacial delamination and debonding between the conductive layer and the compliant polymer substrate [98]. The mechanical mismatch in modulus and strain tolerance generates shear and peel stresses during repeated deformation, driving localized separation, buckling of the conductive film, and stepwise loss of electrical continuity [82].

3.3.1. Spinning

In spinning processes, conductive fillers dispersed within the solution or composite are preferentially aligned along the fiber axis, primarily due to the shear stress imposed as the material passes through the constricted nozzle or spinneret and is subsequently subjected to drawing. Such alignment significantly contributes to enhancing the initial electrical conductivity, as it facilitates the formation of more continuous conductive pathways along the fiber direction [99,100].

Spinning processes can be categorized into wet spinning, electrospinning, and melt spinning. Among these methods, wet spinning is considered advantageous for its simple and intuitive process, which does not require sophisticated equipment [101]. During wet spinning, polymer solutions undergo solidification in a coagulation bath, and the process is significantly influenced by the interdiffusion rate between the solvent and the coagulation medium, which is governed by the solute concentration (i.e., viscosity) as well as the differences in solubility parameters among the solute, solvent, and coagulation medium [102]. Extensive research efforts have aimed at fabricating SCFs with various structures by systematically tuning these parameters [103–106]. For instance, Chen et al. produced a SCF composed of a porous graphene/SBS composite via wet spinning, where SBS acted as the solute, THF served as the solvent, and ethanol was used as the coagulation medium (Fig. 5a [107]. At an SBS concentration of 20 wt%, the fibers formed a porous structure, whereas at a higher concentration of 40 wt%, a dense structure was obtained due to increased viscosity and polymer chain entanglement, which slowed the interdiffusion rate between solvent–coagulation medium. The fabricated porous fiber demonstrated a fracture strain up to 1000 % and a high GF of above 1×10^4 under 0–100 % strain range. In addition, Wu et al. fabricated porous fibers via wet spinning and subsequently coated them with a MXene solution to obtain SCF. In the wet-spinning process, PU was used as the solute, DMF

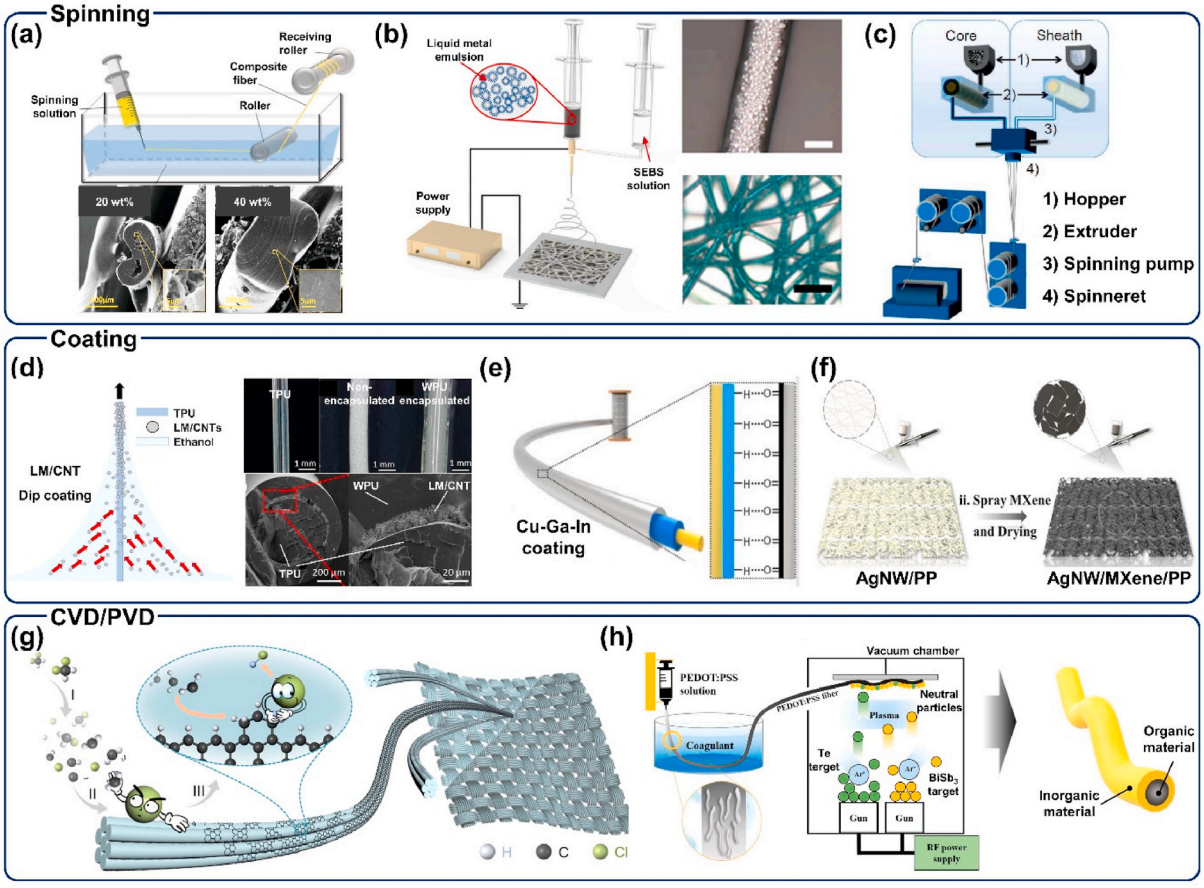

Fig. 5. Fabrication process for SCFs. a-c) Spinning; d-f) Coating, g-f) Chemical/physical vapor deposition (CVD/PVD). a) Schematic diagram of the wet-spinning process and SEM images of fiber morphology with respect to SBS content. Reproduced with permission from ref 107. Copyright 2020 Wiley. b) Coaxial emulsion electrospinning of liquid metal microfibers, and OM image of a microfiber, scale bar: 20 μm; and OM image of fiber mat, scale bar: 200 μm. Reproduced with permission from ref 111. Copyright 2025 Wiley. c) Schematic illustration of the melt-spinning process for SCF fabrication, showing the main components including hopper, extruder, spinning pump, and spinneret. Reproduced with permission from ref 112. CC BY 3.0. d) Schematic diagram of the dip-coating process and surface/cross-section SEM images of SCFs with and without WPU coating. Reproduced with permission from ref 117. Copyright 2025 ACS. e) Bonding mechanism of Cu-Ga-In coated SCF, showing the interfacial adhesion occurring between the gallium oxide layer and PU. Reproduced with permission from ref 118. Copyright 2020 Elsevier. f) Schematic illustration of the fabrication process of the AgNW/MXene 3D conductive network via spray coating. Reproduced with permission from ref 120. Copyright 2021 ACS. g) Schematic of the graphene CVD growing process on glass fiber fabric with dichloromethane as the precursor. Reproduced with permission from ref 123. CC BY 4.0. h) Schematic illustration of fabrication method of the SCF applicable to thermoelectric device: wet-spinning, co-sputtering, and a hybrid thermoelectric fiber Reproduced with permission from ref 127. Copyright 2025 Elsevier.

as the solvent, and a water/ethanol mixture as the coagulation medium. When the ethanol content in the coagulation bath was 20–40 vol%, heterogeneous porous structures with sizes of several hundred micrometers were observed, whereas increasing the ethanol content to >60 vol% led to the formation of homogeneous porous structures on the order of a few micrometers. This phenomenon occurred because increasing the ethanol fraction in the coagulation bath reduced the solubility parameter difference between the solvent and the non-solvent, thereby slowing down the diffusion rate. As a result, fibers with heterogeneous porous structures exhibited a fracture strain of about 1500 %, while those with homogeneous porous structures achieved a high fracture strain of 2865 %. FEA revealed that this difference arose because, in homogeneous porous structures, pores deformed uniformly under strain, allowing stress to be evenly dispersed and thereby enhancing stretchability, whereas heterogeneous porous structures with large pore sizes caused uneven deformation between pores, leading to stress concentration and premature fracture. The resulting homogeneous porous fibers coated with MXene exhibited an initial conductivity of 55.79 S/m [108].

Electrospinning is a simple yet effective technique for fabricating fibers on the micro- and nanoscale. In this process, a polymer solution is extruded under the influence of an electric field, leading to the formation of a Taylor cone at the tip of the spinneret. A Taylor cone is a conical shape formed by the liquid meniscus under an applied electric field, where electrostatic forces deform the fluid into a sharp point, facilitating the ejection of a fine jet [109]. When these electrostatic forces exceed the surface tension of the fluid, a charged jet emerges from the tip of the Taylor cone, which subsequently solidifies into nanofibers [110]. Zhang et al. developed a stretchable conductive nonwoven fabric with a core–shell structure composed of liquid metal and SEBS via electrospinning (Fig. 5b) [111]. They observed that as the flow rate of the liquid metal emulsion increased sequentially, the fiber diameter initially became thicker, but then decreased at higher flow rates. This behavior was attributed to a balance between the volume effect, whereby higher flow rates result in a thicker initial jet, and the stretching effect driven by electrostatic forces within the jet and the external electric field, which act to elongate and thin the jet. The fabricated fabric exhibited a fracture strain exceeding 800 % and a GF of approximately 2.67 under 300 % strain.

Melt spinning is a technique in which conductive composites are heated above their melting points and subsequently extruded through a spinneret. (Fig. 5c). Upon cooling, the extruded material solidifies and is drawn to form continuous fibers. Unlike wet spinning or electrospinning, melt spinning does not involve solvents, making it environmentally friendly, while also offering simplicity and scalability for mass production [112,113]. Cherif et al. utilized melt spinning to produce a SCF based on a composite of CNTs and TPU [114]. The resulting fiber exhibited a fracture strain of 400 %, an initial conductivity of 0.9 S/m, and a gauge factor of 12 within a 50 % strain range.

In terms of industrial readiness, spinning excels in scalability and throughput, as many global synthetic fiber industries have already operated high-volume continuous spinning lines capable of cost-effective and large-scale output [55,115,116].

3.3.2. Coating

Coating methods such as dip coating and spray coating serve as practical approaches to provide electrical conductivity to stretchable polymers. In dip coating, fibers are immersed in a conductive material solution or dispersion, resulting in a direct coating of the conductive layer. This technique is simple and efficient, yet it carries the risk of conductive layer detachment during prolonged use. To address this issue, processing approaches have been proposed to chemically or physically immobilize the conductive layer onto the fiber surface, thereby improving both mechanical and electrical durability. For example, Sheng et al. produced a SCF by immersing TPU fibers in a liquid metal/CNT solution, followed by an additional coating of WPU for encapsulation (Fig. 5d) [117]. The fabricated fiber demonstrated a fracture strain below 300 %, an initial conductivity of 1.15×10^6 S/m, and a GF of 0.5 under 160 % strain. Furthermore, even after 2000 cycles of tensile loading at 50 % strain, the fiber retained excellent reproducibility. Aside from physical encapsulation, chemical strategies to strengthen interfacial interactions between polymers and conductive fillers have been developed. Liu et al. fabricated a core–shell structured SCF by first coating PU fibers with polymethacrylates, then applying a semi-liquid metal (Cu–Ga–In) layer (Fig. 5e) [118]. In this process, polymethacrylates facilitated hydrogen bonding between the semi-liquid metal and the polymer matrix, thus improving adhesion. The fabricated fiber achieved a fracture strain exceeding 300 %, exhibited an initial conductivity as high as 5.2×10^6 S/m and a GF of 2.3 under 0–300 % strain range. Importantly, it maintained stable resistance over 2000 cycles at 100 % strain.

Spray coating is a technique employed to deposit a dispersion of conductive materials onto the surfaces of polymer fibers, enabling uniform coatings and facilitating high production efficiency [13,119]. However, similar to dip coating, the weak interfacial adhesion between the conductive layer and the fiber can lead to a reduction in the mechanical and electrical durability of the SCFs. As an example, aimed at overcoming this, Qu et al. developed SCF by spray-coating surface-modified AgNWs and MXene onto commercial nonwoven fabric. In this process, the C═O groups on AgNWs and terminal groups (–O, –OH, –F) on MXene formed hydrogen bonds, enhancing stability (Fig. 5f) [120]. The fabricated fiber achieved a fracture strain exceeding 600 %, an initial resistance of 6.2 Ω, and a GF of 57.7 under 0–60 % strain range. It also showed stable performance over 1500 cycles at 8 % strain, indicating excellent durability and repeatability.

Regarding industrial readiness, these coating-based fabrication methods enable the conversion of conventional elastic yarns into conductive fibers without redesigning the base polymer system, thereby significantly lowering industrial barriers. In addition, these are inherently compatible with roll-to-roll or yarn-to-yarn continuous manufacturing lines, enabling high throughput and competitive cost [10,12,121]. Consequently, coating-based approaches currently represent a highly viable pathway to large-scale commercialization, combining low infrastructure establishment cost, high processing speed, and proven reliability in real textile environments.

3.3.3. CVD/PVD

CVD for SCFs is a method where gaseous reactants chemically transform to form a conductive layer on polymer surfaces. This technique optimizes the electrical properties of SCFs by adjusting parameters such as reaction time, surface pre-treatment, and precursor selection [13]. Bose et al. developed a SCF by depositing PPy onto electrospun PU fibers via oxidative chemical vapor deposition [122]. The fabricated fiber achieved a fracture strain exceeding 400 %, an initial resistance of 106 kΩ, and a GF of 46 at a strain of 202 %. Nonetheless, one of the limitations of CVD processes is the lengthy deposition time, often ranging from several hours to days, due to the low catalytic activity of the insulator. Recently, Liu et al. introduced a rapid graphene growth technique on glass fibers using dichloromethane as a carbon source, which has a low decomposition energy barrier and generates highly electronegative chlorine radicals, enabling the fabrication of graphene-coated glass fiber fabric (Fig. 5g) [123].

PVD processes, such as thermal evaporation and sputtering, involve vaporizing solid conductive materials and depositing them onto fiber surfaces to generate conductive coatings. In thermal evaporation, metals are heated until vaporized and then condensed onto fiber surfaces to form conductive layers of high purity. By contrast, sputtering involves bombarding a metal target with plasma ions, causing metal atoms to be ejected and deposited uniformly onto fiber surfaces, resulting in coatings with excellent coverage and uniformity [7]. The conductive layer deposited via PVD exhibits high electrical conductivity owing to its high crystallinity, high density, and low defect concentration [124,125]. Liu

et al. fabricated a stretchable conductive non-woven fabric by electrospinning a fluoro rubber-based sheet, followed by gold deposition via sputtering. The resulting sheet exhibited a stretchability exceeding 150 %, a sheet resistance of 17.7 Ω/sq, and a GF of 1.3 under 0–60 % strain [126]. In a similar approach, Han et al. employed wet spinning to produce PEDOT:PSS fibers, which were subsequently coated with bismuth–antimony–telluride through sputtering, yielding conductive fibers with an initial conductivity of 5660 S/m (Fig. 5h) [127].

In terms of industrial applicability, however, CVD-based deposition remains fundamentally limited for mass production of SCFs. Although CVD offers atomically uniform films and robust bonding, the high temperature, vacuum environment, and slow deposition rates present major incompatibilities with most polymeric textile substrates. Only a narrow set of high-temperature fibers can withstand typical CVD conditions, and adapting CVD reactors for continuous processing drastically increases operational costs. Current demonstrations are mostly research-oriented, and no broad commercial deployment exists. Consequently, the industrial readiness of CVD for SCFs remains low despite its exceptional material quality. Similar to CVD, PVD-based fabrication is technologically mature but only partly transferable to SCFs. Although PVD enables low-temperature deposition of thin conductive layers, the 3-dimensional morphology of yarns can induce shadowing effects and nonuniform coating, leading to crack formation under strain. In addition, even though the cost and reliability constraints reduce its suitability for scalable manufacturing, PVD can be configured for continuous processing and could be viable for specific advanced purposes.

4. Applications for SCFs

SCF-based E-textiles naturally conform to the human body, offering comfortable wearability. Furthermore, they possess excellent breathability, effectively mitigating skin irritation problems that commonly arise from prolonged use of traditional wearable electronic devices [128, 129]. This section reviews recent studies investigating the application potential of SCFs in various fields, including stretchable bio-electrodes, sensors, heaters, displays, and energy harvesters.

4.1. Bio-electrodes

SCF-based E-textiles show significant promise as bio-electrodes for continuous monitoring of bioelectric signals during daily activities without causing discomfort. To enable such applications, the electrodes must adhere well to the skin, maintain high electrical conductivity, and exhibit minimal resistance changes during stretching [130]. Previous studies on SCFs have reported their use as bioelectrodes for measuring bioelectric signals such as the electrocardiogram (ECG), electroencephalogram (EEG), and electromyogram (EMG), which respectively

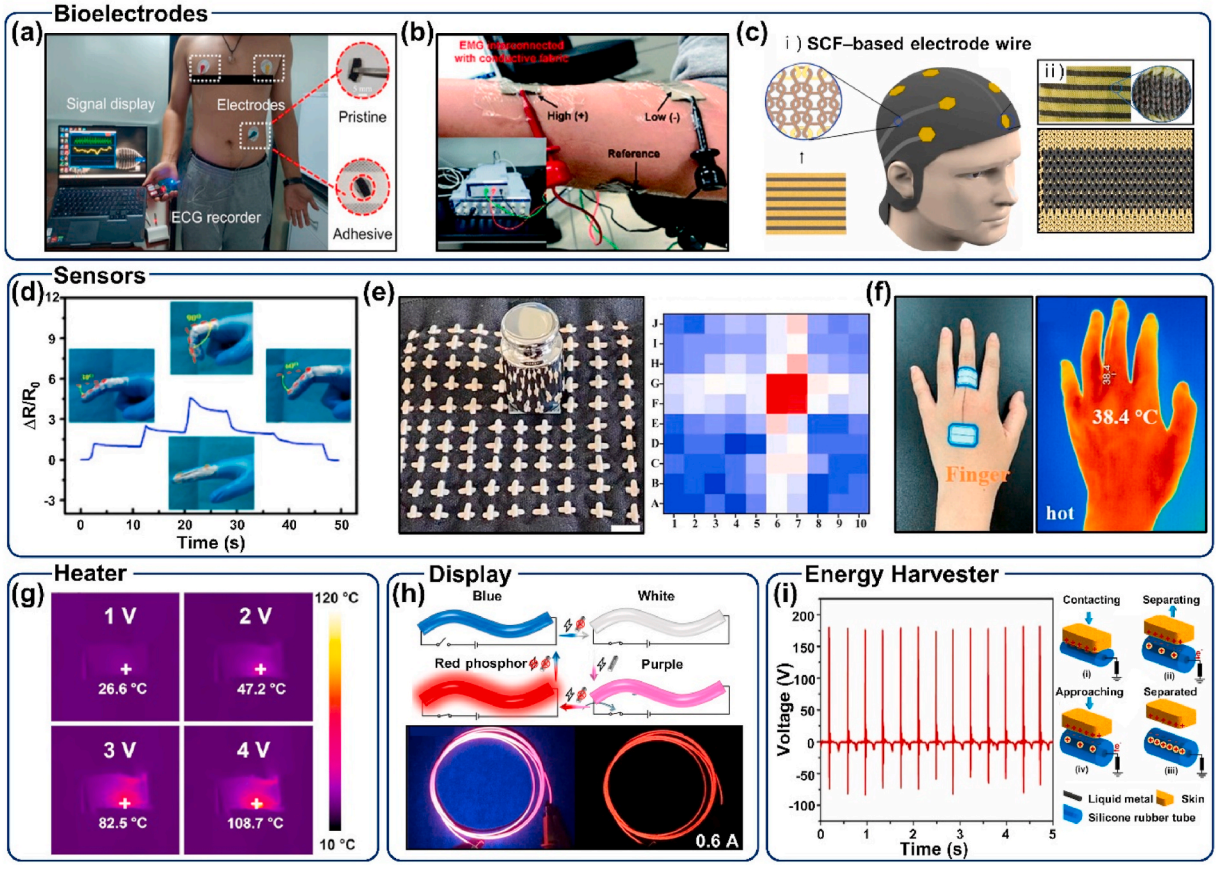

Fig. 6. Applications of SCFs. a-c) Bioelectrodes: a) Hydrogel-based SCF utilized as a bio-electrode for ECG monitoring. Reproduced with permission from ref 134. Copyright 2024 Wiley. b) Bio-electrodes for EMG signal monitoring composed of silver-based stretchable conductive textiles. Reproduced with permission from ref 136. CC BY-NC 3.0. c) EEG measurement cap integrating nickel-based SCF electrodes. Reproduced with permission from ref 138. Copyright 2025 Elsevier. d-f) Sensors: d) Human motion detection of SCF: finger bending to 0°, 30°, 60° and 90°. Reproduced with permission from ref 142. Copyright 2024 Elsevier. e) SCFs based 10 × 10 sensing array and capacitance change ratio of the sensor array versus pixel location. Reproduced with permission from ref 147. Copyright 2024 ACS. f) Performance of the SCF-based temperature sensor applied on a hand. Reproduced with permission from ref 151. Copyright 2024 Elsevier. g) Joule heating performances of the SCF based textile under different voltages. Reproduced with permission from ref 158. Copyright 2022 ACS. h) Schematic diagram of the excitation mechanism and image of glowing SCFs under joule heating and UV irradiation. Reproduced with permission from ref 164. Copyright 2024 Wiley. i) Voltage signals of the SCF-based TENG and working mechanism. Reproduced with permission from ref 171. Copyright 2022 Elsevier.

monitor the electrical activity of the heart, brain, and muscles.

ECG measures variations in cardiac electrical potentials by placing electrodes at multiple sites on the body. This technique noninvasively detects depolarization of cardiac muscle, enabling diagnosis of abnormal heart rhythms [131]. Conventional ECG electrodes, such as Ag/AgCl gel-type patches, may cause skin irritation and impair skin breathability [132]. To address these issues, recent efforts have therefore focused on developing ECG electrodes using SCFs. Liu et al. fabricated a three-layer all-nanofiber-based PTFE, AgNWs, and a silk fibroin nanofiber membrane fabric electrode via electrospinning [133]. This fabric electrode exhibited a low sheet resistance (~3.58 Ω/sq) and a high-water vapor transmission rate (2553 g m^{-2} d^{-1} at 35 °C), demonstrating better breathability than commercial Ag/AgCl gel electrodes. The electrode was subsequently employed to fabricate ECG electrodes capable of clearly capturing distinct waveforms, including the P, Q, R, S, and T waves. Wang et al. similarly developed a hydrogel-based SCF with a fracture strain exceeding 200 % and an initial conductivity of 192.7 S/m (Fig. 6a) [134]. SCF-based fiber electrodes attached to the chest were employed to measure ECG signals, and the acquired signals were wirelessly transmitted through Bluetooth modules and displayed on a PC or smartphone for diagnostic analysis. In addition, to assess the biocompatibility of the fiber for direct skin applications, in vivo studies on mouse and human skin confirmed no irritation over 72 h, demonstrating skin compatibility comparable to commercial Ag/AgCl electrodes and similarly effective ECG signal acquisition.

EMG is used to measure and evaluate electrical signals generated in skeletal muscles during voluntary or involuntary contractions and relaxations [130]. Zhu et al. created a stretchable ionic gel conductive fiber by wet spinning a composite of cellulose nanofibers and PVA [135]. The fiber achieved a fracture strain of 627 %, an initial conductivity of 0.54 S/m, and a GF of 2.79 at 100 % strain. Electrodes fabricated from this SCF successfully detected EMG signals corresponding to finger movements. Son et al. developed a stretchable conductive textile by immersing PU fabrics in Ag-based ink (Fig. 6b) [136]. To evaluate its capability for physiological signal detection, the conductive fabric was integrated into an EMG monitoring system by configuring three MED-ET interconnections: reference, active (+), and ground (−). These electrodes were conformally attached to the skin using a transparent Tegaderm patch, enabling stable acquisition of EMG signals. This textile showed a low GF of 0.12 under 0–300 % strain range and was employed for monitoring EMG signals from the forearm flexor muscles, accurately detecting muscle contractions.

EEG is a noninvasive technique for recording electrical signals generated by neural activity, useful for assessing consciousness, sleep quality, and diagnosing neurological disorders. Liu et al. fabricated a stretchable conductive fiber comprising SEBS, Ag, and EGaIn via electrospinning and coating [137]. The sheet exhibited a high stretchability of approximately 1000 % and a GF of 0.4 under 400 % strain. When utilized for electroencephalography (EEG) measurements, it effectively distinguished α signals recorded with eyes open versus closed. In addition, Bagherzadeh et al. developed a SCF on flexible polyimide through nickel electroless plating (Fig. 6c) [138]. To fabricate an SCF-based EEG cap, PET yarn and the SCF were integrated using a double-layer weft--knitted structure, resulting in a textile electrode configuration suitable for EEG acquisition. The fiber maintained a low resistance below 4 Ω under strain up to 110 %. This fiber was integrated into an EEG measurement cap, achieving performance comparable to conventional EEG caps.

4.2. Wearable sensors

Deformable sensors can detect various movements and physiological changes of the wearer or the surrounding environment, converting these physical and chemical stimuli into electrical signals [139]. SCFs, which possess excellent mechanical and electrical performance, can be embedded within garments or textiles to act as sensing elements, allowing real-time monitoring of bodily motions and physiological parameters [140]. Depending on their sensing mechanisms, SCFs can be applied as various types of sensors, including strain, pressure, temperature, and humidity sensors.

Strain sensors operate on a principle whereby mechanical deformation or external stress modifies the conductive pathways within the material. In particular, mechanical strain increases the tunneling distance between adjacent conductive regions, resulting in a rise in electrical resistance. Upon release of the strain, the conductive pathways restore to their initial state [141]. A variety of studies have investigated the fabrication of SCFs for strain-sensing applications. Shen et al. produced a porous SCF composed of MWCNT, reduced graphene oxide, and TPU through a wet spinning process (Fig. 6d) [142]. The resulting fiber demonstrated a fracture strain of 686 %, an initial resistance of 75.1 kΩ, and a GF of 300 under 120 % strain. To evaluate motion monitoring, an electrode layer was prepared by coating both ends of the SCF with silver paste and copper tape, and this layer was then attached to the wearer's body. This fiber was demonstrated as a strain sensor capable of detecting motion across various body regions, including the fingers, wrists, elbows, and knees.

Pressure sensors operate by detecting mechanical pressure and converting into corresponding electrical signals, and are classified into piezoresistive, piezoelectric, triboelectric, and capacitive types according to their fundamental sensing principles [143]. Recent studies have targeted the use of SCF-based pressure sensors for monitoring physiological signals, including pulse rate, blood pressure, acoustic vibrations, and intraocular pressure [144–146]. For examples, Lv et al. developed a porous SCF by employing wet spinning to produce hollow TPU/sodium chloride (NaCl) fibers, followed by the removal of NaCl and subsequent injection of liquid metal into the resulting central void [147]. The SCF exhibited a fracture strain of 450 % and exhibited a GF of 3.32 within a strain range of 0–250 %. Utilizing this fiber, they fabricated a capacitive-type pressure sensor with a sensitivity of 0.2493 kPa^{-1}, which is higher than that of non-porous SCFs (0.0455 kPa^{-1}). By weaving the SCFs with cotton–linen fabric as warp threads, a cross-grid E-textile incorporating a 10 × 10 sensor array was demonstrated, enabling the detection and mapping of locally applied pressure (Fig. 6e).

Temperature sensors are essential for monitoring and measuring temperature in diverse settings. When incorporated into E-textile platforms, they enable functions such as continuous body temperature monitoring, sweat detection, early identification of infections, and prevention of thermal injuries [148]. SCF-based temperature sensors operate on the principle that conductive materials exhibit changes in electrical resistance with temperature fluctuations, following either a negative temperature coefficient (NTC) or positive temperature coefficient (PTC) response [149]. These sensors deliver enhanced flexibility and stretchability compared to traditional temperature sensors, permitting direct integration into textiles while minimizing discomfort during wear [150]. Piao et al. fabricated a SCF by coating spandex polyurethane fibers with a hybrid composite of polyaniline-L-cysteine ethyl ester hydrochloride (PANI-LCO) and AgNWs. The fiber exhibited a fracture strain exceeding 1000 %, a high initial conductivity of 2.7 × 10^2 S/m, and a GF of 14.63 at 60 % strain. (Fig. 6f) [151]. Moreover, the introduction of PANI-LCO effectively reduced the junction resistance of AgNWs, leading to the high performance of the PANI-LCO-AgNW/SP temperature sensor, which exhibited a high temperature coefficient of resistance (TCR) of up to 47.4 %/°C. Using the SCF-based temperature sensor, which was attached to the hand, human body temperature changes were evaluated by immersing the hand in ice and hot water, with the sensor exhibiting an average TCR of 10.4 %/°C in the temperature range of 31.8–38.4 °C.

Humidity sensors are crucial for accurately detecting the moisture content in various environments. When integrated into E-textiles, such sensors enable applications ranging from real-time skin hydration monitoring and respiration tracking to managing humidity levels within garments to enhance wearer comfort [152]. The operating principles of

humidity sensors are classified into chemical and physical adsorption. In chemical adsorption, water molecules bind to hydrophilic conductive surfaces, whereas in physical adsorption, moisture layers form on the fiber surface. By these adsorption behaviors, the resistance, capacitance, or impedance of SCFs is altered, thereby enabling humidity sensing [153]. Xin et al. developed a conductive fiber sheet through electrospinning of Zinc oxide (ZnO) NPs/polyvinylidene fluoride (PVDF) composites, followed by in situ polymerization of PANI onto the fiber surfaces [154]. The fabricated fiber sheet exhibited a fracture strain exceeding 30 % and an initial resistance of 9.01 kΩ. This material was subsequently employed to fabricate a humidity sensor that demonstrated high sensitivity and fast response time of 38 s under humid conditions, signifying reliable and stable humidity detection. The sensing mechanism relies on chemical adsorption, where water molecules interact with PANI and facilitate the abstraction of protons (H^+) from amino groups (-NH_2). This allows the lone pair electrons on nitrogen atoms to resonate with the phenyl groups along the PANI backbone, effectively enhancing electron delocalization and thereby modulating the electrical properties of the sensor.

4.3. Wearable heaters

Wearable heaters are designed to regulate body temperature and safeguard individuals in extreme environmental conditions. Their operation primarily depends on Joule heating, a phenomenon where electrical energy is transformed into heat as current passes through conductive materials [155,156].

SCFs possess superior flexibility and stretchability, making them suitable for wearable heater applications. When integrated into textile structures, they maintain wearer comfort and deliver efficient thermal insulation. Importantly, these fibers can conform to complex body geometries while consistently sustaining heating performance, offering practical value for military cold-weather apparel and medical therapeutic devices [155]. Zhang et al. fabricated a SCF by wet-spinning process using coaxial needle, in which polyurethane (PU) formed the shell and GaInSn served as the core [157]. The resulting core-shell structured fiber exhibited a fracture strain exceeding 300 %, an initial conductivity of 3.4×10^6 S/m, and a low GF of 3.1 under 200 % strain. When the SCF was used as a heating element in wearable applications, it exhibited stable thermal output that increased proportionally with the applied voltage, reaching 39.2 °C at 0.1 V and 85.2 °C at 0.6 V. Similarly, Yu et al. developed a SCF based on a composite of MXene, liquid metal, and SBS (Fig. 6g) [158]. The SCF showed a fracture strain greater than 500 %, an initial conductivity of 3.923 S/m, and a GF of approximately 0.33 under 300 % strain. To fabricate a wearable heater, the SCFs were first woven, after which copper electrodes were connected to both ends using silver paste. The wearable heater incorporating this fiber achieved a temperature rise to 26.6 °C at 1 V and reached 103.7 °C under 4 V, demonstrating robust heating capabilities.

4.4. Wearable displays

Wearable displays can be directly integrated on human body, enabling real-time visual output and communication through light emission [159,160]. Early implementations involved attaching rigid LEDs to fabrics, resulting in devices that were bulky and thick, thereby diminishing the drapability and washability of textiles [161]. In contrast, displays constructed from SCFs are lightweight and capable of deforming in synchrony with human motion. These systems can adhere to skin or integrate into garments while preserving wearer comfort and fabric flexibility [162]. For SCF-based displays to operate reliably under mechanical deformation, high luminance and high current efficiency at low operational voltages are critical requirements [163]. Jin et al. developed a core–shell SCF via wet spinning using liquid metal and polyacrylonitrile [164]. The SCF showed a fracture strain exceeding 20 % and an initial resistance of 3.7 Ω. Moreover, by incorporating luminescent materials and thermochromic pigments into the shell layer during fabrication, color changes in response to temperature variations can be enabled. Upon applying a current of 0.6 A, color shifts were observed due to Joule heating effects in the liquid metal core (Fig. 6h). A wearable display was fabricated by weaving the SCFs into a textile structure. The display based on such SCFs not only enabled pressure detection through electrical signals but also induced color changes corresponding to the location and intensity of the applied pressure, thereby allowing pressure visualization. The pressure sensor based on such SCFs not only enabled pressure detection through electrical signals but also induced color changes corresponding to the location and intensity of the applied pressure, thereby allowing pressure visualization. Peng et al. constructed a woven display by combining ionic liquid/PU-based conductive weft fibers produced via melt spinning and Ag-based warp fibers coated with ZnS-based phosphors [165]. At the intersections of weft and warp, electroluminescent units were formed. When voltage was applied, an electric field was established between the conductive weft and luminescent warp, causing electron excitation within the ZnS phosphor doped with Cu or Mn, followed by photon emission as the electrons relaxed to the ground state. The device exhibited a luminance of approximately 115 cd/m^2 under an operational electric field of 3.7 V/μm at 2000 Hz.

4.5. Wearable energy harvesters

Energy harvesting technologies transform diverse environmental energy sources, including human motion, thermal gradients, and vibrations, into electrical energy, which is particularly valuable for powering E-textiles and wearable electronics where continuous energy supply is limited [166,167]. Activities such as breathing, fluctuations in body temperature, blood circulation, arm movement, typing, and walking can collectively produce power outputs exceeding 100 W, positioning them as viable sources of sustainable energy [168]. SCF-based energy harvesters can be seamlessly integrated into textiles, offering stable power to E-textiles without frequent battery charging while preserving flexibility and breathability for user comfort [6,169].

In recent studies on SCF-based energy harvesters, the triboelectric and piezoelectric effects have often been employed. The triboelectric effect describes contact-induced charge transfer between two materials of different positions in the triboelectric series, while the piezoelectric effect converts mechanical deformation of piezoelectric materials into electrical energy via polarization-induced potential differences [170]. Hao et al. fabricated a core–shell SCF based on GaInSn and silicone rubber via dry-spinning, achieving a fracture strain exceeding 300 % and maintaining a GF of 0.31 under 130 % strain (Fig. 6i). [171] The SCF-based energy harvester was fabricated by weaving the fibers in a warp–weft configuration, in which the liquid alloy contained in the central channel functioned as the electrode, while the surrounding silicone-rubber fiber network acted as the insulating and frictional layer. Using the SCF, they developed a triboelectric nanogenerator (TENG) achieving an output voltage of 175 V and a power density of 469 mW/m^2. Meanwhile, Kuo et al. fabricated a SCF from SBS and AgNPs via electrospinning, achieving a fracture strain of 711.85 % and a GF of approximately 0.31 at 150 % strain [172]. Combining PVDF and AgNWs, they developed a nanogenerator delivering a piezoelectric voltage of 29.5 V, a current of 0.39 μA, and a power output of 11.57 μW.

5. Quantitative trend analysis of SCFs

A total of 124 studies published during the past decade were summarized in Table S1 for the quantitative trend analysis of the mechanical and electrical properties of SCFs, including the maximum work strain, the GF_{avg}, and initial conductivity. It should be noted that the maximum work strain is defined as the highest strain at which variations in resistance are detectable, representing the effective stretchability of SCFs to sustain functional electrical responses. Most SCFs exhibited

maximum work strains ranging from several tens to over 1000 %, indicating that they possess the minimum stretchability required for potential application in E-textiles. In addition, in this analysis, the GF_{avg} was defined as the maximum ratio of resistance variation (Max. $\Delta R/R_0$) divided by the maximum work strain to conduct a comprehensive and fair comparison across previous SCF studies, which utilized different strain ranges when reporting their GFs.

Based on Table S1, an investigation was conducted to examine how the structural and material designs influence the key performance properties of SCFs, as illustrated in Figs. 7–9. Furthermore, the characteristic features of SCFs applied to specific application fields were extracted, as illustrated in Fig. 10. After that, the cyclic stretchability of SCFs was also discussed. To derive reliable insights from numerous references, various materials and structural designs were systematically classified and treated as independent variables.

5.1. *Effect of structural design on performance of SCFs* 173–211

Fig. 7 provides a comprehensive overview of structural design effects on SCFs, classified by the types of conductive materials. Across all material types, SCFs without structural engineering, referred to as 'Dense' (Black squares in Fig. 7), exhibited relatively higher GF_{avg} compared with SCFs incorporating specific structural designs. This can be attributed to the fact that in the absence of engineered structural features, the applied strain is directly transferred to the conductive network, thereby amplifying the relative resistance changes under deformation. In other words, the lack of structural accommodation mechanisms causes even small tensile strains to induce significant perturbations in the conductive pathways through filler–filler separation, tunneling-distance expansion, and microcrack initiation within the matrix etc., leading to enhanced strain sensitivity and, consequently, higher GF_{avg} values [39].

In contrast, SCFs with structural designs such as helical, serpentine, or wrinkle configurations (Blue triangles, green inverted triangles, and purple diamonds in Fig. 7, respectively) consistently demonstrated significantly lower GF_{avg}. The reduced GF_{avg} in these cases reflects the fundamental role of structural engineering in mitigating strain-induced disruptions within the conductive network. Specifically, these engineered geometries provide intrinsic mechanical compliance: wrinkles unfold, serpentine patterns elongate, and helices extend in response to

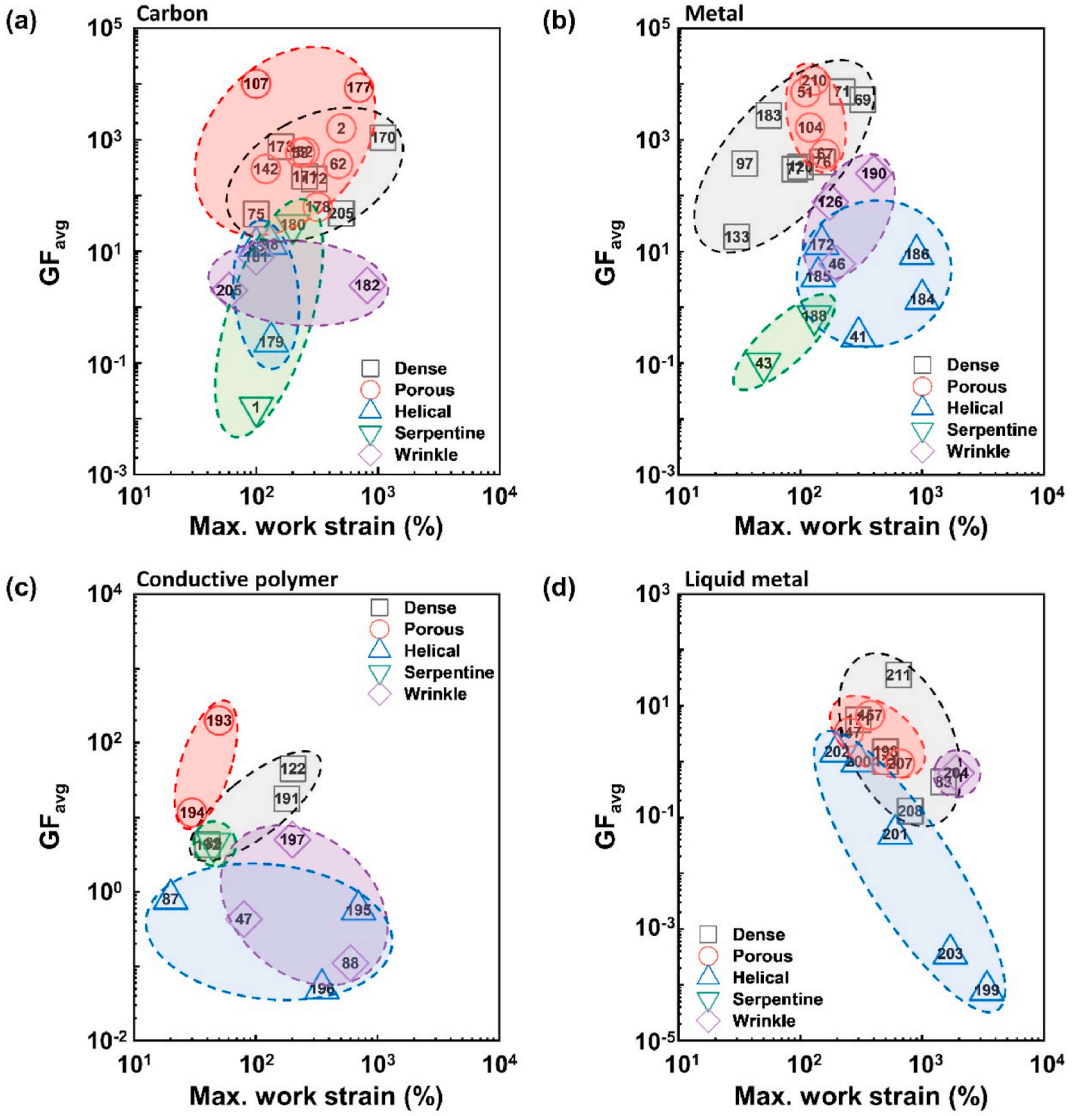

Fig. 7. Effect of structural design on performance of SCFs compared in terms of GF_{avg} versus maximum work strain: Structural designs, including dense, porous, helical, serpentine, and wrinkle, are distinguished within each material category; a) Carbon-based, b) Metal-based, c) Conductive polymer-based, and d) Liquid metal-based SCFs. The values of GF_{avg} are defined as the maximum ratio of $\Delta R/R_0$ divided by the maximum work strain. The reference data from the research conducted over the past 10 years are provided in Table S1 of the Supplementary Materials.

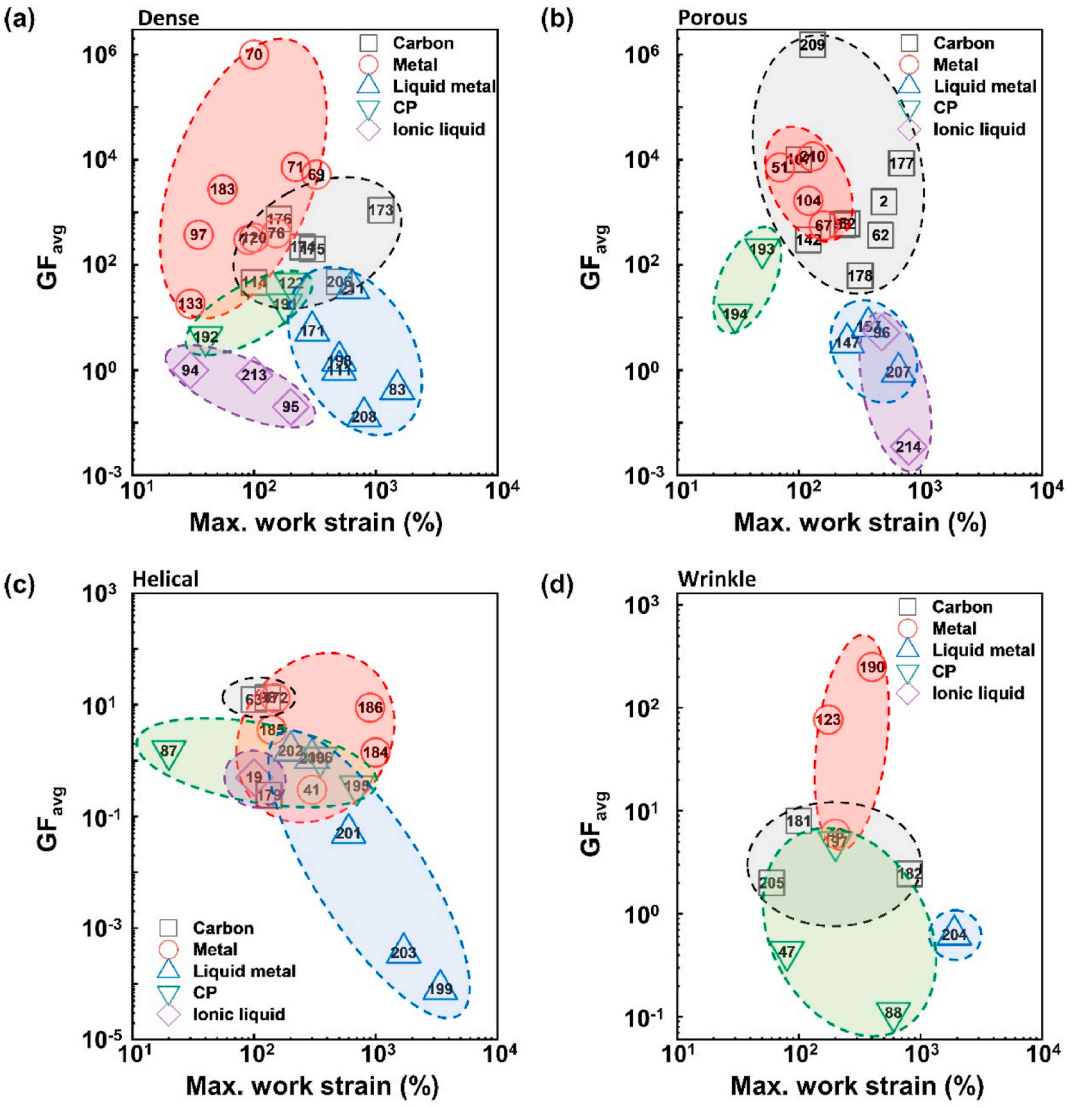

Fig. 8. Effect of material type on performance of SCFs compared in terms of GF_{avg} versus maximum work strain: Materials including carbon, metals, liquid metals, conductive polymers (CP), and ionic liquids, are distinguished within each structural category; a) Dense, b) Porous, c) Helical, and d) Wrinkle structured SCFs. The values of GF_{avg} are defined as the maximum ratio of $\Delta R/R_0$ divided by the maximum work strain. The reference data from the research conducted over the past 10 years are provided in Table S1 of the Supplementary Materials.

external strain. Such deformation mechanisms enable the material to accommodate mechanical stretching through geometric rearrangements rather than through substantial displacement of conductive fillers [1]. This strain-decoupling effect stabilizes the percolation network by limiting filler–filler separation, suppressing tunneling-distance changes, and delaying microcrack initiation within the matrix [40]. As a result, the inter-filler distance remains relatively stable during stretching, and the resistance variation is minimized, thereby yielding lower GF_{avg} values. In particular, the serpentine structure exhibited a maximum work strain of only about 200 %, whereas the wrinkle and helical structures demonstrated a much broader range of maximum work strains depending on the material type. This difference arises because the helical architecture employs a three-dimensional curved form, and the wrinkle structure allows flexible adjustment of the pre-strain level, while the serpentine structure relies on a planar curved form. Separately, while these structured SCFs offer clear advantages in achieving high stretchability, their unconventional geometries could raise some challenges about how readily they can be integrated with conventional textile fibers with dense structures and whether they can feasibly transition into commercial applications.

In contrast to SCFs with other structural designs, SCFs with porous structures generally exhibited high GF_{avg}, comparable to that of dense SCFs. This behavior can be ascribed to the fact that the presence of pores alters the way strain is distributed within the material. When SCFs are stretched, the applied strain is not evenly dispersed but is instead concentrated around the pore boundaries. This localized strain concentration induces a pronounced separation between conductive fillers, thereby causing a significant increase in the inter-filler distance. Such microstructural deformation enhances the sensitivity of the SCFs to strain, leading to higher GF_{avg} values. Furthermore, in the porous structure, lower initial conductivity was observed in carbon- and metal-based SCFs, which is primarily attributed to the extension and disruption of electrical pathways within the conductive network (Fig. S1). In porous configurations, the conductive channels are elongated and more tortuous, which increases the overall resistance of the system. As a result, the initial conductivity decreases because the electrons encounter a longer and more resistive percolation path before achieving stable conduction. Exceptionally, porous SCFs incorporating liquid metals exhibited high initial conductivity, which is considered to result from the superior intrinsic conductivity of liquid metals. Collectively, these

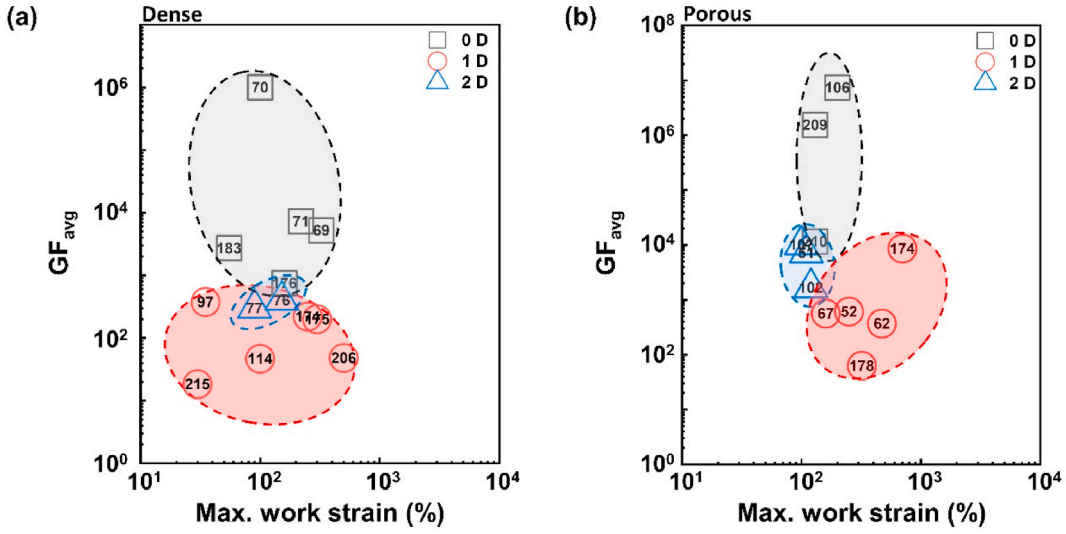

Fig. 9. Effect of material dimensionality on performance of SCFs compared in terms of GF_{avg} versus maximum work strain: effects of material dimension on SCF performance are distinguished within each structural category; a) Dense, b) Porous. The values of GF_{avg} are defined as the maximum ratio of $\Delta R/R_0$ divided by the maximum work strain. The reference data from the research conducted over the past decade are provided in Table S1 of the Supplementary Materials.

effects highlight the dual role of porous structures in simultaneously enhancing strain sensitivity while compromising initial conductivity.

5.2. *Effect of material type on performance of SCFs [96,212–214]*

Fig. 8 presents a quantitative analysis of the effects of conductive material types employed in SCFs. Regardless of the structural design, SCFs based on carbon and metal materials (Black squares and red circles in Fig. 8, respectively) consistently exhibited higher GF_{avg}. than those utilizing other materials, such as liquid metals, conductive polymers, and ionic liquids (Blue triangle, green inverted triangles, and purple diamonds in Fig. 8, respectively). This is attributed to the intrinsic physical properties of the conductive materials incorporated into or onto SCFs. As is well known, carbon and metal materials possess high elastic moduli, which hinder them from conforming well to the deformation of the polymer matrix [22,215]. On the other hand, liquid metals, conductive polymers, and ionic liquids are extremely soft and deformable, enabling them to accommodate matrix deformation with minimal disturbance to the conductive pathways [19,216]. As a result, SCFs incorporating these soft materials generally exhibit lower GF_{avg} values while maintaining stable electrical responses under large strains.

In terms of initial conductivity, metal- and liquid-metal-based SCFs exhibited higher values than those of other material systems due to their intrinsically high conductivity (Fig. S2). Unexpectedly, carbon-based SCFs showed the lowest initial conductivity, despite the superior intrinsic conductivity of carbon, which is even comparable to that of ionic-liquid-based SCFs. This behavior is likely due to severe filler aggregation caused by π–π interactions among the conjugated structures of carbon nanomaterials, such as carbon nanotubes and graphene. Even when partial dispersion is achieved, these strong interactions hinder the establishment of a well-connected and continuous conductive network within the polymer matrix, thereby limiting the effective conductivity at the initial state. All conductive materials exhibit a trade-off in which higher initial conductivity corresponds to lower GF_{avg} (Fig. S3). This trend is consistent with percolation behavior in conductive composites: as the filler network becomes more densely connected, the initial conductivity increases, but the network also becomes less sensitive to small mechanical perturbations. In such tightly percolated systems, strain-induced changes in inter-filler distance or tunneling pathways remain minimal until a relatively large deformation is applied, resulting in smaller variations in resistance and consequently lower GF values. To summarize, these observations emphasize that material selection is a dominant factor influencing the initial conductivity and GF_{avg}.

5.3. *Effect of material dimensionality on performance of SCFs*

Conductive materials used in SCFs, particularly carbon, metal, and MXene, exhibit distinct characteristics depending on their morphological dimensionality, classified as zero-dimensional (0D), one-dimensional (1D), and two-dimensional (2D). 0D conductive materials are spherical particles typically sized between 1 and 10 nm, with prominent examples including CB and metallic nanoparticles such as AuNPs and AgNPs [217]. 1D conductive materials, such as CNTs and AgNWs, possess significantly higher aspect ratios compared to 0D materials, enabling SCFs to reach a lower percolation threshold even with reduced filler loading. This property is advantageous for achieving low elastic modulus and enhanced stretchability in SCFs [13,177]. 2D conductive materials, such as graphene, MXene, and metallic nanoflakes, consist of one or multiple atomic layers, with each layer held together by non-covalent interactions such as van der Waals forces [218,219].

Han et al. developed SCFs based on carbon materials with different dimensionalities. The fibers containing CB within polymer matrices experienced a substantial decrease in conductivity upon stretching, whereas those containing 1D materials (e.g., MWCNTs) maintained better conductivity under similar deformation [173]. This result is strongly substantiated by Fig. 9, which quantitatively illustrates the impact of conductive filler dimensionality on the electrical and mechanical properties. SCFs incorporating 0D conductive materials (Black squares in Fig. 9) exhibit higher GF_{avg} than those employing 1D or 2D materials (Red circles and blue triangles in Fig. 9, respectively). This behavior, particularly evident in the cases of dense and porous structures, originates from the intrinsic characteristics of 0D materials, which possess smaller particle sizes and lower aspect ratios, making SCFs utilizing 0D fillers more vulnerable to the disruption of conductive networks under mechanical strain and leading to a pronounced increase in resistance and, in turn, higher GF_{avg} [173].

In contrast, SCFs incorporating 1D or 2D conductive materials generally exhibit lower GF_{avg}, a trend that directly arises from the intrinsic continuity and mechanical robustness of their filler networks. 1D materials such as CNTs and nanowires form elongated, interlocking percolation pathways that maintain electrical connectivity through sliding, rotation, and partial reorientation under strain, thereby suppressing abrupt resistance changes. Likewise, 2D materials provide

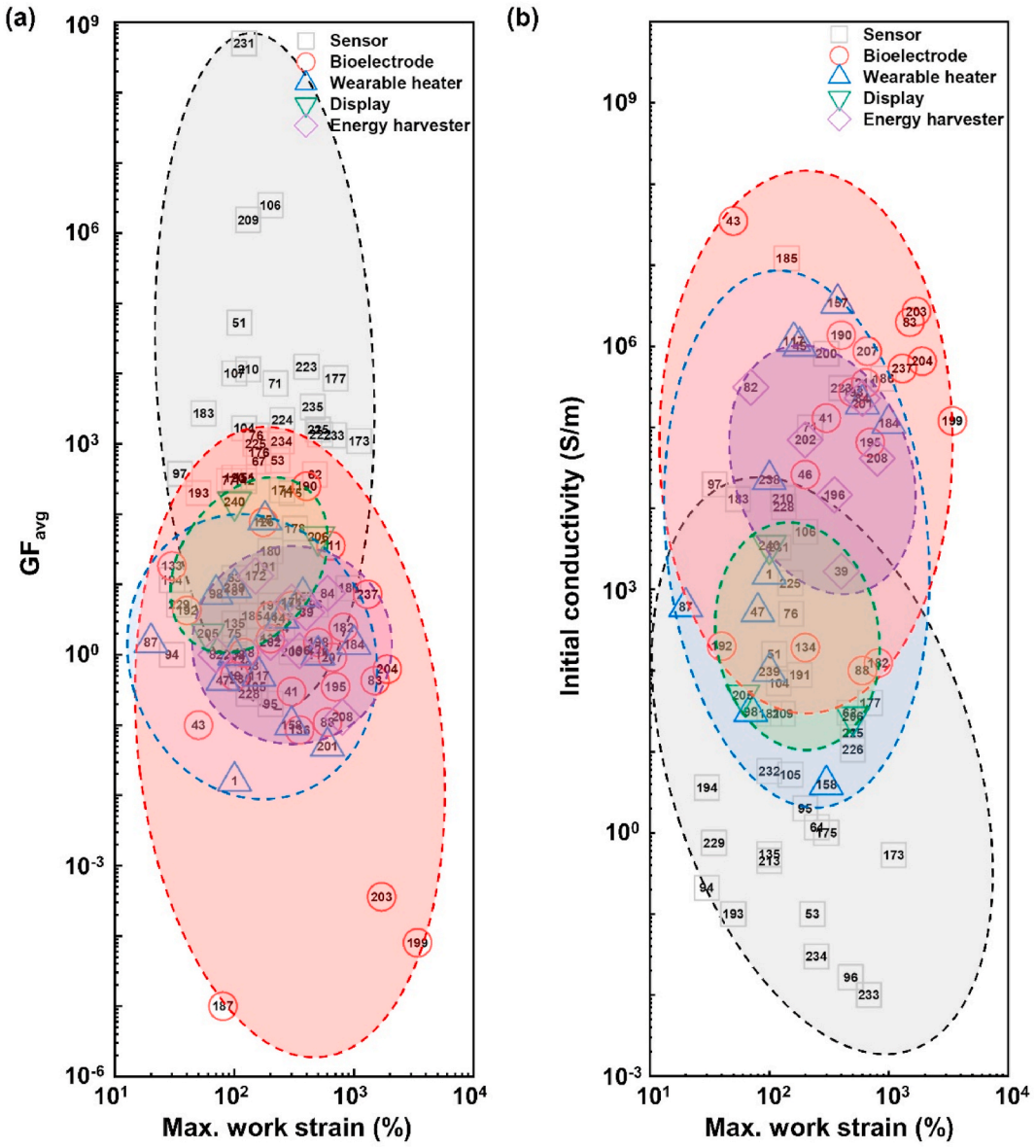

Fig. 10. Application comparison of SCFs based on GF_{avg}, initial conductivity, and maximum work strain. a) Maximum work strain vs. GF_{avg}. The values of GF_{avg} are defined as the maximum ratio of $\Delta R/R_0$ divided by the maximum work strain. b) Maximum work strain vs. initial conductivity. The reference data from the research conducted over the past decade are provided in Table S1 of the Supplementary Materials.

broad contact areas and overlapping networks that preserve conductive pathways even when subjected to substantial deformation. The resulting low GF_{avg} values indicate high electrical stability under dynamic strain conditions for wearable applications, where consistent signal acquisition or stable current delivery must be maintained despite continuous body motion. While 2D fillers typically result in SCFs with a maximum work strain limited to around 100 %, SCFs using 1D fillers exhibit a much broader range of maximum work strains. This broader variability arises not only from differences in percolation behavior but also from the ability of 1D materials to form diverse and mechanically compliant conductive pathways, such as interlocking, entangled, or partially aligned networks, combined with the versatility of fabrication processes used to assemble them [173].

However, the implications of material dimensionality were not observed in SCFs with helical and serpentine structures. In the case of the helical structure, this absence can be explained by the fact that the GF_{avg} values were exceedingly low, and the variations among them were negligible, making it difficult to draw any meaningful correlations with the dimensionality of the conductive materials. For serpentine and wrinkled structures, the lack of observable implications is likely related to the limited number of previous studies that have specifically investigated this configuration. Because only a small body of research is available, the dataset is insufficient to establish consistent trends or to quantitatively evaluate the role of dimensionality.

5.4. Cyclic stretchability of SCFs

We analyzed the cyclic stretchability reported in each paper using strain and strain cycles serving as essential indicators for evaluating durability under realistic use conditions. To clarify the trends, we plotted the reported SCFs based on the two parameters. In most reported studies, cyclic durability of SCFs has been demonstrated under repeated deformation with applied strains up to ~100 % and cycling numbers reaching ~10,000. Given that conventional textile fibers are typically evaluated using only a limited number of high-strain tensile cycles, SCFs undergo far more extensive cyclic testing [220]. This reflects the

research trend of positioning SCFs not merely as textiles but as components for next-generation wearable electronic devices, aligning with durability parameter used in commercial foldable mobile devices, which are tested up to hundreds of thousands of cycles [221]. Only a limited number of SCFs have been evaluated beyond 20,000 cycles or at stretch ratios exceeding 200 %. Notably, no study has simultaneously explored both extreme conditions, indicating a clear trade-off between achievable strain and cycle number.

From a fabrication-process perspective, SCFs produced via spinning or coating methods consistently exhibit substantially higher stretchability and cyclic durability than those fabricated using PVD or CVD techniques (Fig. S4a). While most PVD- and CVD-based SCFs typically exhibited cyclic stretching only up to ~50 % strain and fewer than ~5000 cycles, spinning-based SCFs commonly showed the stretchability of 100 % with stable electrical performance over ~10,000 cycles. Coating-based SCFs further demonstrate robust stretchability even under more extreme strain and prolonged cyclic loading conditions. This superior cyclic stretchability originates from the intrinsic structural compliance of spinning- and coating-derived structures, in which conductive networks are either embedded within or conformally integrated with elastomeric matrices, enabling distributed stress accommodation and delayed crack initiation, whereas PVD- and CVD-derived SCFs rely on thin, stiff surface-deposited conductive layers that are prone to interfacial stress concentration, microcracking, and delamination under repeated large deformation. From a structural perspective, SCFs tested above ~20,000 cycles adopt stretchable architectures such as helical or porous designs (Fig. S4b). This indicates that accommodating applied strain through geometric rearrangement or stress-buffering voids is crucial for mitigating fatigue damage accumulation [51]. Differences in cyclic stretchability across material types were not significant (Fig. S4c). When comparing filler dimensionality, SCFs with 1D fillers were generally tested at higher strain and higher cycles than those using 0D and 2D fillers, consistent with their inherently higher stretchability with diverse and mechanically compliant conductive pathways (Fig. S4d).

Most studies do not report the failure point of cyclic stretchability, thus the reported strains do not necessarily reflect the true performance limits of each SCF. For this reason, we also extracted the relative strain normalized to the maximum work strain in a single tensile loading (Table S1 in the Supplementary Materials). The relative strain implies the SCFs' potential cyclic durability capacity, which has not yet been fully realized or demonstrated in existing studies. We found that most SCFs were tested at less than 50 % of the relative strain, indicating that their durability claims are typically evaluated under conservative loading conditions (Fig. S5)

5.5. Application-specific characteristics of SCFs [222-240]

The performance requirements of SCFs differ substantially depending on their application fields, and the relative importance of GF_{avg} and initial conductivity also varies accordingly. GF_{avg} characterizes the strain sensitivity of SCFs, whereas initial conductivity is closely associated with its ability to deliver stable electrical signals. Maximum work strain implies the mechanical stretching range of SCFs for each application field. Therefore, an appropriate balance between GF_{avg} and initial conductivity with sufficiently high work strain is essential for optimizing SCFs for specific functions.

Fig. 10 summarizes the GF_{avg}, initial conductivity and maximum work strain of SCFs reported in previous studies, categorized according to their application fields. Most SCFs exhibit a maximum work strain in the range of 100–1000 %, reflecting the requirement that all wearable-device applications should remain functional under the large deformations caused by human motion and body bending. Characteristically, SCFs developed for bio-electrode and wearable heaters (Red circles and blue triangles in Fig. 10, respectively) exhibited relatively low GF_{avg} and high initial conductivity. This trend likely reflects the need to maintain stable current flow under continuous body motion, which is particularly important for reliable bio-signal acquisition and for achieving steady, uniform heating in wearable heater applications. Likewise, SCFs developed for wearable energy harvesters (Purple diamonds in Fig. 10) showed a similar trend, which may be due to the necessity of achieving high short-circuit currents and efficient energy conversion, along with the requirement for low GF_{avg} to minimize unnecessary resistance fluctuations during repetitive mechanical motions.

In contrast, SCFs used for sensors (Black squares in Fig. 10) generally exhibit high GF_{avg} and low initial conductivity, unlike those used in bioelectrodes, wearable heaters, or energy harvesters. This is because high strain sensitivity requires the initial conductivity to be set near the point where electrical resistance changes most sharply with strain. Wearable displays (Green inverted triangle in Fig. 10), on the other hand, commonly employ SCFs with moderate GF and initial conductivity to ensure stable and uniform device operation. Understanding these distinctions offers critical guidance for the rational design of SCFs and supports their integration into next-generation wearable and soft electronic systems.

6. Challenges and outlook

Despite substantial advances in materials development, structural design, and fabrication strategies for SCFs, several critical challenges remain unresolved before their practical integration into textile systems can be fully realized. In particular, long-term durability and user-related considerations under realistic operating conditions have not yet been sufficiently addressed. This section therefore discusses several key unresolved issues, including wash durability, biocompatibility, chemical stability under environmental exposure, and dyeability, which fundamentally limit the practical adoption of SCFs. Addressing these challenges in a systematic and application-oriented manner will be essential for bridging the gap between laboratory-scale demonstrations and industrial-scale implementation.

6.1. Wash durability

Wash durability refers to the ability of SCFs to maintain their electrical performance, mechanical integrity, and structural morphology after repeated laundering cycles, which inherently involve water immersion, detergent exposure, mechanical agitation, and temperature fluctuations during washing and drying. Unlike conventional textile products, wash durability in SCFs entails more stringent requirements. it must ensure not only the preservation of mechanical properties and appearance but also the stability of continuous conductive pathways under coupled chemical, mechanical, and thermal stresses. As a result, wash durability directly governs long-term reliability, user safety, and consumer acceptance, and thus represents a critical prerequisite for commercialization [241].

Despite its importance, current wash durability evaluations for SCFs remain highly fragmented, as summarized in Table S2. Testing approaches reported in the literature range from simple water immersion to mechanically intensified protocols employing stirring or ultrasonic agitation. Some studies incorporate detergents to enhance chemical stress, whereas others rely on household washing machines to approximate real-use conditions. Washing durations and cycle numbers vary widely from a few minutes to several hours or even months of exposure, and from a single cycle to more than 200 cycles. Moreover, the selection of testing standards is inconsistent, with studies referencing AATCC 61, AATCC 135, ISO 6330, JIS L1930, GB/T 3921-2008, or adopting non-standardized procedures.

Such variability underscores the absence of a unified framework for evaluating wash durability in SCFs, complicating cross-study comparisons and obscuring meaningful performance benchmarks. More critically, although real laundering inherently involves not only exposure to water and detergents but also thermal fluctuations during drying

processes, the effects of thermal cycling and drying-induced thermal stress on the electrical and mechanical stability of SCFs remain largely unexplored. This omission represents a significant gap in current durability assessments.

From a broader perspective, this gap highlights the urgent need for standardized, multidimensional testing frameworks that move beyond simplified or purely accelerated laundering models. As critically discussed by Rotzler and co-workers, the diversity of washability tests in E-textiles reflects not methodological flexibility but rather the absence of a coherent evaluation framework that links laboratory protocols to realistic use conditions. Future wash durability assessments for SCFs should therefore capture the coupled and sequential nature of laundering, in which chemical exposure, mechanical agitation, and thermal cycling interact synergistically throughout washing and drying processes [242].

In parallel, performance metrics must be explicitly defined with respect to electrical functionality, including acceptable thresholds for resistance drift, signal stability, and electrical failure modes under repeated laundering. Equally important, standardized protocols should be aligned with realistic usage scenarios, such as expected washing frequency, service lifetime, and end-use categories, to ensure industrial relevance. Establishing harmonized benchmarks along these lines will be essential not only for enabling meaningful cross-study comparisons but also for bridging the gap between laboratory-scale demonstrations and industrial validation of wash-durable SCFs [243].

6.2. Biocompatibility

Biocompatibility refers to the ability of SCFs to operate without eliciting adverse biological responses, including cytotoxicity, skin irritation, and sensitization, as well as electrical and physicochemical side effects such as leakage current, conductive particle shedding, and harmful electrochemical reactions upon contact with skin or bodily environments. As SCFs are directly integrated into wearable and textile-based electronic systems, biocompatibility constitutes a fundamental prerequisite for commercialization, governing user safety, regulatory acceptance, and reliable long-term wearability under repeated mechanical deformation and prolonged skin contact.

To address these concerns, extensive research efforts have explored material-, structure-, and process-level strategies to improve the biocompatibility of SCFs. Representative approaches include the use of intrinsically biocompatible materials, such as liquid metals and hydrogels, to reduce the biological risks associated with rigid metallic conductors or brittle conductive coatings [199,200,230]. Structurally, electrospinning-based fabrication has enabled highly porous fibrous architectures that enhance air permeability and moisture transport, thereby alleviating skin occlusion and irritation during continuous wear [126]. In addition, microfluidic encapsulation strategies have been developed to confine conductive components within sealed elastomeric channels, effectively preventing conductive particle leakage and unintended exposure of electrical pathways to the surrounding tissue environment [196]. Several studies have further validated these designs through in vivo assessments using rodent models, demonstrating stable bio-signal acquisition without observable tissue damage, inflammation, or abnormal immune responses [105,135].

Nevertheless, most reported biocompatibility assessments remain limited to proof-of-concept demonstrations and are weakly connected to regulatory evaluation frameworks. Wearable E-textiles are not developed in a regulatory vacuum. Depending on their intended use, they are already subject to existing standards and guidelines that explicitly or implicitly define biocompatibility requirements. Consequently, SCFs, as core functional components of E-textile systems, should be designed, fabricated, and evaluated with these frameworks in mind.

For medical device–oriented applications involving prolonged or repeated skin contact, E-textiles are expected to comply with the risk-based biological evaluation framework defined in ISO 10993-1. This framework requires standardized assessment of cytotoxicity, skin irritation, and sensitization, often supported by alternative non-animal testing methods such as OECD Test Guideline 439, which evaluates skin irritation using reconstructed human epidermis models. However, many existing studies rely on simplified cytotoxicity assays or limited in vivo observations, which are insufficient to demonstrate compliance with regulatory-grade biocompatibility requirements. For consumer-grade applications such as sportswear and outdoor apparel, E-textile are expected to comply with textile safety frameworks rather than medical biocompatibility standards. In this context, OEKO-TEX® Standard 100 is adoptable to certify chemical safety and skin compatibility by restricting harmful substances in E-textile products intended for direct skin contact. At the same time, international standardization activities led by IEC/TC 124 are actively defining safety, reliability, and performance requirements for wearable electronic systems, underscoring that E-textiles are increasingly subject to formalized technical standards.

Therefore, although substantial progress has been made in improving the intrinsic biocompatibility of SCFs through material innovation and structural design, the lack of systematic, regulation-aligned evaluation strategies remains a critical barrier to industrial adoption [244]. To enable meaningful translation from laboratory research to commercial products, future studies must move beyond material-centric demonstrations and explicitly incorporate standardized biocompatibility assessments aligned with existing E-textile and wearable regulations [245].

6.3. Chemical stability

Chemical stability describes the ability of SCFs to retain their electrical and mechanical performance, as well as structural integrity, when exposed to chemically aggressive environments such as human sweat, variable pH conditions, detergents, and outdoor pollutants. Sweat-derived salts, acids, and organic compounds, together with washing surfactants and alkaline solutions, can accelerate corrosion, hydrolysis, swelling, and interfacial delamination of SCFs [223,227]. Consequently, achieving chemical stability comparable to that of commercially established textile products is essential to ensure reliable long-term performance under realistic wear and laundering conditions.

To mitigate chemical degradation, various material- and structure-driven strategies have been proposed. These include fluorinated polymer-based waterproof coatings that act as hydrophobic and chemically inert barriers [223], soft elastomeric encapsulation layers such as Ecoflex that combine hydrophobicity, chemical stability, and mechanical compliance [227], and core–shell fiber architectures that physically isolate conductive cores from external chemical stimuli [207]. In addition, strengthening the interfacial interactions between conductive fillers and polymer matrices via tailored surface functionalization has been shown to suppress conductive particle detachment and preserve interfacial integrity under chemically challenging conditions [77].

Despite these advances, chemical stability has predominantly been evaluated under simplified laboratory conditions. For practical deployment in wearable and textile-based applications, chemical stability of SCFs must be systematically evaluated under well-defined chemical stress conditions that emulate actual wear scenarios, including exposure to artificial sweat, repeated laundering processes, and long-term environmental weathering.

Accordingly, standardized chemical stability evaluations should be incorporated to reflect realistic use conditions of SCF-based E-textiles. In particular, artificial sweat exposure tests based on ISO 105-E04 provide a practical framework to assess the resistance of SCFs to sweat-induced chemical stress during prolonged skin contact. Although originally developed for color fastness evaluation, this standard offers a chemically relevant environment that can be extended to monitor changes in electrical performance and structural integrity of SCFs. In addition, chemical durability under repeated laundering, evaluated using ISO 6330 and AATCC 61, is critical for SCFs intended for wearable and

textile applications [243]. These standards simulate detergent exposure and washing-induced chemical stress under controlled conditions, enabling systematic assessment of performance retention and failure modes associated with repeated washing cycles [241].

In addition to sweat and laundering, weathering resistance constitutes a critical yet often overlooked component of chemical stability for SCF-based E-textiles intended for outdoor and daily-use applications. Although no standardized test methods have been specifically established for evaluating the weathering resistance of SCFs or E-textiles, these systems ultimately function as textile products exposed to sunlight, temperature fluctuations, humidity, and atmospheric pollutants. Accordingly, well-established weathering standards originally developed for conventional textiles offer the most practical evaluation frameworks, even though they were not explicitly designed for conductive fibers. Textile-based standards such as the ISO 105-B series for light fastness and the accelerated aging protocols defined in the ISO 4892 series, together with weathering test methods specified in AATCC TM16, AATCC TM169, and ASTM G154 and G155, have been widely used to evaluate the environmental durability of fibers, fabrics, and coated textiles under simulated outdoor conditions.

While these standards do not directly address electrical functionality, their application to SCF-based systems enables systematic investigation of photo-induced and environment-driven chemical degradation processes, including polymer oxidation, embrittlement, and interfacial deterioration, which can directly compromise conductive pathways and encapsulation layers. Therefore, adapting existing textile weathering standards to SCF-based E-textiles, coupled with concurrent monitoring of electrical and mechanical performance, represents a rational and necessary approach for evaluating long-term chemical stability in the absence of SCF-specific regulations.

6.4. Dyeability

A significant challenge lies in exploiting adequate dyeability in SCFs. Color, as a visual parameter, has a profound impact on human perception, emotional response, garment aesthetics, initial consumer interest, and ultimately, purchasing behavior [246]. As a result, dyeability is a critical factor that determines the practical usability and commercial prospects of SCFs-based E-textiles, particularly for specialized applications such as military uniforms, where color precision and vibrancy are essential [247]. However, SCFs constructed from carbon-based or metallic materials often exhibit inherently dark hues, leading to low lightness values even after dyeing processes. Furthermore, ensuring that mechanical and electrical properties remain stable during dyeing introduces additional technical complexity [24]. Consequently, advancing the integration of SCFs into conventional textile dyeing workflows demands innovative strategies focused on both improving the durability of these fibers and enhancing their dyeability through structural and materials engineering [246,248,249].

7. Conclusion

This review has provided a comprehensive overview of SCFs, focusing on structural designs and conductive materials as the primary factors governing their mechanical and electrical properties, while also outlining representative fabrication techniques and highlighting potential applications. Detailed discussions have also been included on the characteristics of different structural configurations, the intrinsic properties of the materials employed, and the fundamental principles of processing methods.

In particular, based on studies reported over the past decade, we quantitatively analyzed how the structural designs of SCFs and the conductive materials incorporated into them influence GF and initial conductivity. Furthermore, we extracted the generalizable characteristics of GF and initial conductivity associated with potential application fields as presented in previous studies. These systematic evaluations not only provide more accurate perspectives on the current state of SCFs but also are expected to serve as guiding principles for future SCF research and technological advancement.

Future research will likely focus on enhancing the functional performance of SCFs while concurrently addressing the essential requirements of wash durability, biocompatibility, chemical stability, and dyeability. Progress in this field will depend on multidisciplinary collaborations that bridge traditional textile engineering with advanced materials science, nanotechnology, and chemical processing, paving the way for practical, safe, and commercially viable E-textile.

Declaration of competing interest

The authors declare that they have no known competing financial interests or personal relationships that could have appeared to influence the work reported in this paper.

Acknowledgments

This work was supported by the Basic Science Research Program through the National Research Foundation of Korea (NRF), funded by the Ministry of Education (RS-2022-NR075810). This work was also supported by the Korea Institute for Advancement of Technology (KIAT) under a grant funded by the Ministry of Trade, Industry & Energy (MOTIE) (RS-2024-00409639, HRD Program for Industrial Innovation), as well as by the Korea Planning & Evaluation Institute of Industrial Technology (KEIT) (RS-2024-00420537), funded by MOTIE. In addition, this work was supported by the Fundamental Research Program (PNKA630) of the Korea Institute of Materials Science (KIMS).

Appendix A. Supplementary data

Supplementary data to this article can be found online at https://doi.org/10.1016/j.jmrt.2025.12.232.

Data availability

The data that support the findings of this study are available from the corresponding author, G. Y. Bae, upon reasonable request.

References

[1] Yuan H, Jia R, Yao H, Wang W, Qian K, Wu X, et al. Ultra-stable, waterproof and self-healing serpentine stretchable conductors based on WPU sheath-wrapped conductive yarn for stretchable interconnects and wearable heaters. Chem Eng J 2023;473:1–10.
[2] Li W, Liu J, Wei J, Yang Z, Ren C, Li B. Recent progress of conductive hydrogel fibers for flexible electronics: fabrications, applications, and perspectives. Adv Funct Mater 2023;33:1–28.
[3] Wu Y, Mechael SS, Carmichael TB. Wearable E-Textiles using a textile-centric design approach. Acc Chem Res 2021;54:4051–64.
[4] Zhang Y, Wang H, Lu H, Li S, Zhang Y. Electronic fibers and textiles: recent progress and perspective. iScience 2021;24:1–20.
[5] Gonçalves C, da Silva AF, Gomes J, Simoes R. Wearable E-Textile technologies: a review on sensors, actuators and control elements. Inventions 2018;3:1–13.
[6] Zeng W, Shu L, Li Q, Chen S, Wang F, Tao XM. Fiber-based wearable electronics: a review of materials, fabrication, devices, and applications. Adv Mater 2014;26:5310–36.
[7] Zhang Y, Zhang Y, Zhou J, Zhang D, Lin H, Chen Y, et al. Stretchable composite conductive fibers for wearables. Adv Mater Technol 2023;8:1–25.
[8] Zhu C, Wu J, Yan J, Liu X. Advanced fiber materials for wearable electronics. Adv Fiber Mater 2022;5:12–35.
[9] Al-Oqla FM, Sapuan SM, Anwer T, Jawaid M, Hoque ME. Natural fiber reinforced conductive polymer composites as functional materials: a review. Synth Met 2015;206:42–54.
[10] Zhang W, Miao J, Zuo X, Zhang X, Qu L. Weaving a magnificent world: 1D fibrous electrodes and devices for stretchable and wearable electronics. J Mater Chem C 2022;10:14027–52.
[11] Wang B, Facchetti A. Mechanically flexible conductors for stretchable and wearable E-Skin and E-Textile devices. Adv Mater 2019;31:1–53.
[12] Lee J, Llerena Zambrano B, Woo J, Yoon K, Lee T. Recent advances in 1D stretchable electrodes and devices for textile and wearable electronics: materials, fabrications, and applications. Adv Mater 2019;31:1–53.

[13] Song X, Ji J, Zhou N, Chen M, Qu R, Li H, et al. Stretchable conductive fibers: design, properties and applications. Prog Mater Sci 2024;144:1–31.
[14] Takasaki H, Aoki M, Muraki T, Uchiyama E, Murakami G, Yamashita T. Muscle strain on the radial wrist extensors during motion-simulating stretching exercises for lateral epicondylitis: a cadaveric study. J S E S 2007;16:854–8.
[15] Jung D, Kim S-Y, Sohn A, Jeon B-Y, Kim S-Y, Lee J-Y. Regional skin maximal elongation rate for appling E-Textiles to tight-fit clothing. Korean J Community Living Sci 2017;28:365–75.
[16] Gao J, Wang X, Zhai W, Liu H, Zheng G, Dai K, et al. Ultrastretchable multilayered fiber with a hollow-monolith structure for high-performance strain sensor. ACS Appl Mater Interfaces 2018;10:34592–603.
[17] Persons AK, Ball JE, Freeman C, Macias DM, Simpson CL, Smith BK, et al. Fatigue testing of wearable sensing technologies: issues and opportunities. Mater 2021;14:1–27.
[18] Chen R, Xu X, Yu D, Xiao C, Liu M, Huang J, et al. Highly stretchable and fatigue resistant hydrogels with low young's modulus as transparent and flexible strain sensors. J Mater Chem C Mater 2018;6:11193.
[19] Chen S, Liu H, Liu S, Wang P, Zeng S, Sun L, et al. Transparent and waterproof ionic liquid-based fibers for highly durable multifunctional sensors and strain-insensitive stretchable conductors. ACS Appl Mater Interfaces 2018;10:4305–14.
[20] Eom J, Jaisutti R, Lee H, Lee W, Heo JS, Lee JY, et al. Highly sensitive textile strain sensors and wireless user-interface devices using all-polymeric conducting fibers. ACS Appl Mater Interfaces 2017;9:10190–7.
[21] Kayser LV, Lipomi DJ. Stretchable conductive polymers and composites based on PEDOT and PEDOT: PSS. Adv Mater 2019;31:1–13.
[22] Lund A, Wu Y, Fenech-Salerno B, Torrisi F, Carmichael TB, Müller C. Conducting materials as building blocks for electronic textiles. MRS Bull 2019;46:491–501.
[23] Huang X, Liu L, Lin YH, Feng R, Shen Y, Chang Y, et al. High-stretchability and low-hysteresis strain sensors using origami-inspired 3D mesostructures. Sci Adv 2023;9:1–11.
[24] Agcayazi T, Chatterjee K, Bozkurt A, Ghosh TK. Flexible interconnects for electronic textiles. Adv Mater Technol 2018;3:1–32.
[25] Won C, Cho S, Jang KI, Park JU, Cho JH, Lee T. Emerging fiber-based neural interfaces with conductive composites. Mater Horiz 2025;12:4545–72.
[26] Ojstršek A, Plohl O, Gorgieva S, Kurečič M, Jančič U, Hribernik S, et al. Metallisation of textiles and protection of conductive layers: an overview of application techniques. Sensors 2021;21:1–28.
[27] Huang F, Hu J, Yan X. Review of fiber-or yarn-based wearable resistive strain sensors: structural design, fabrication technologies and applications. Textiles 2022;2:81–111.
[28] Wu X, Han Y, Zhang X, Lu C. Highly sensitive, stretchable, and wash-durable strain sensor based on ultrathin conductive layer@ polyurethane yarn for tiny motion monitoring. ACS Appl Mater Interfaces 2016;8:9936–45.
[29] Taherian R. Development of an equation to model electrical conductivity of polymer-based carbon nanocomposites. ECS Journal of Solid State Sci Technol 2016;3:26–38.
[30] Lee J, Shin S, Lee S, Song J, Kang S, Han H, et al. Highly sensitive multifilament fiber strain sensors with ultrabroad sensing range for textile electronics. ACS Nano 2018;12:4259–68.
[31] Liu Y, Tang Y, Guo X, Qu L, Liu Y, Zhang X, et al. Template-free and stretchable conductive fiber with a Built-In helical structure for strain-insensitive signal transmission. ACS Appl Mater Interfaces 2023;15:46379–87.
[32] Zhou CG, Sun WJ, Jia LC, Xu L, Dai K, Yan DX, et al. Highly stretchable and sensitive strain sensor with porous segregated conductive network. ACS Appl Mater Interfaces 2019;11:37094–102.
[33] Oh J, Yang JC, Kim JO, Park H, Kwon SY, Lee S, et al. Pressure insensitive strain sensor with facile solution-based process for tactile sensing applications. ACS Nano 2018;12:7546–53.
[34] Zhu L, Zhang W, Luan S, Wei J, Yang Y, Miao J. Nanomaterials for smart wearable fibers and textiles: a critical review. iScience 2025:1–18.
[35] Lee S, Jaseem SA, Atar N, Wang M, Kim JY, Zare M, et al. Connecting the dots: sintering of liquid metal particles for soft and stretchable conductors. Chem Rev 2025;125:3551–85.
[36] Lu W, Wu G, Gan L, Zhang Y, Li K. Functional fibers/textiles for smart sensing devices and applications in personal healthcare systems. Anal Methods 2024;16:5372–90.
[37] Hou S, Chen C, Bai L, Yu J, Cheng Y, Huang W. Stretchable electronics with strain-resistive performance. Small 2024;20:1–43.
[38] Spinks GM. Advanced actuator materials powered by biomimetic helical fiber topologies. Adv Mater 2020;32:1–13.
[39] Wang M, Chen Z, Dong L, Wu J, Li C, Gao Q, et al. Conductance-Stable and integrated helical Fiber Electrodes toward stretchy energy storage and self-powered sensing utilization. Chem Eng J 2023;457:1–11.
[40] Hou K, Shi X, Yuan J, Zhang D, Bai Y, Xu J, et al. Stretchable PU@CNT/mXene fiber fabricated by external tension for high performance strain sensor and supercapacitor. Adv Mater Technol 2023;8:1–11.
[41] Yu B, Gu Q, Hu G, Yang T, Liu M, Shi H, et al. A reduction-driven directed aggregation strategy for fabricating stretchable conductive core-sheath fibers in wearable electronics. Chem Eng J 2024;480:1–11.
[42] Shi Y, Zhao J, Zhang B, Qin J, Hu X, Cheng Y, Yu J, Jie J, Zhang X. Freestanding serpentine silicon strips with ultrahigh stretchability over 300% for wearable electronics. Adv Mater 2024;36:2313603.
[43] Jiang C, Li Q, Fan S, Guo Q, Bi S, Wang X, et al. Hyaline and stretchable haptic interfaces based on serpentine-shaped silver nanofiber networks. Nano Energy 2020;73:1–10.
[44] Pandurangi SS, Kulkarni SS. Mechanics of wrinkling of a thin film bonded to a compliant substrate under the influence of spatial thermal modulation. Int J Solids Struct 2015;62:124–33.
[45] Lee J, Kim DW, Chun S, Song JH, Yoo ES, Kim JK, et al. Intrinsically strain-insensitive, hyperelastic temperature-sensing fiber with compressed micro-wrinkles for integrated textronics. Adv Mater Technol 2020;5:1–10.
[46] Yoon K, Lee S, Shim D, Lee M, Cho S, Kwon C, et al. Strain-insensitive stretchable fiber conductors based on highly conductive buckled shells for wearable electronics. ACS Appl Mater Interfaces 2023;15:18281–9.
[47] Li Y, Shan M, Peng J, Lan L, Wei L, Guo L, et al. A highly stretchable and conductive continuous composite filament with buckled polypyrrole coating for stretchy electronic textiles. Appl Surf Sci 2023;610:1–10.
[48] Peng W, Liu Y, Wang C. Definition, measurement, and function of pore structure dimensions of bioengineered porous bone tissue materials based on additive manufacturing: a review. Front Bioeng Biotechnol 2023;10:1–16.
[49] Liu J, Li H, Li H, Song W, Xia S, Wei D, et al. Deep-sea glass sponges-like hollow porous ceramic fiber aerogel: fabrication, anti-shrinkage and thermal insulation. Ceram Int 2024;50:37714–25.
[50] Zhao B, Li X, Gu C, Wang Y, Liu H, Guo X, et al. Highly stretchable and strain sensitive MXene/MXene: mwcnts@ TPU fiber with hierarchical conductive layers and porous elastic core structure. Colloids Surf, A Physicochem Eng Asp 2024;690:1–9.
[51] Guo Q, Pang W, Xie X, Xu Y, Yuan W. Stretchable, conductive and porous MXene-Based multilevel structured fibers for sensitive strain sensing and gas sensing. J Mater Chem A Mater 2022;10:15634–46.
[52] Gu C, Qin W, Wang Y, Li X, Wang J, Tian Z, et al. Highly stretchable, durable, and superfine fiber-shaped strain sensor with a porous core-sheath microstructure. Compos Commun 2022;36:1–7.
[53] Sheng N, Ji P, Zhang M, Wu Z, Liang Q, Chen S, et al. High sensitivity polyurethane-based fiber strain sensor with porous structure via incorporation of bacterial cellulose nanofibers. Adv Electron Mater 2021;7:1–12.
[54] Wang X, Zheng S, Xiong J, Liu Z, Li Q, Li W, et al. Stretch-induced conductivity enhancement in highly conductive and tough hydrogels. Adv Mater 2024;36:2313845.
[55] Zhu S, Huang Y, Fang B. Progress and prospect for conducting polymer fibers. Adv Mater 2025:e04071.
[56] Rehman A, Zeng X. Ionic liquids as green solvents and electrolytes for robust chemical sensor development. Acc Chem Res 2012;45:1667–77.
[57] Zhu J, Li J, Tong Y, Hu T, Chen Z, Xiao Y, et al. Recent progress in multifunctional, reconfigurable, integrated liquid metal-based stretchable sensors and standalone systems. Prog Mater Sci 2024;142:101228.
[58] Li X, Chen S, Peng Y, Zheng Z, Li J, Zhong F. Materials, preparation strategies, and wearable sensor applications of conductive fibers: a review. Sensors 2022;22:1–30.
[59] Wang R, Sun L, Zhu X, Ge W, Li H, Li Z, et al. Carbon nanotube-based strain sensors: structures, fabrication, and applications. Adv Mater Technol 2022;8:1–31.
[60] Chen W, Cai M, Wu J, Ma H, Liu W, Xu F. Highly conductive, durable, washable, and scalable composite yarn for multifunctional wearable electronic applications. Compos Sci Technol 2023;241:1–9.
[61] Zhang S, Zhao B, Zhang D, Yang M, Huang X, Han L, et al. Conductive hydrogels incorporating carbon nanoparticles: a review of synthesis, performance and applications. Particuology 2023;83:212–31.
[62] Zeng J, Ma W, Wang Q, Yu S, Innocent MT, Xiang H, et al. Strong, high stretchable and ultrasensitive SEBS/CNTs hybrid fiber for high-performance strain sensor. Compos Commun 2021;25.
[63] Huang F, Hu J, Yan X. A wide-linear-range and low-hysteresis resistive strain sensor made of double-threaded conductive yarn for human movement detection. J Mater Sci Technol 2024;172:202–12.
[64] Zhu W, Wang S, Lu Y, Yang W, Ge S, Lou Z, et al. High-toughness multifunctional conductive hydrogel fibers via microfluidic spinning for flexible strain sensor. Ind Crop Pro 2024;222:1–11.
[65] Tehrani M. Advanced electrical conductors: an overview and prospects of metal nanocomposite and nanocarbon based conductors. Phys Status Solidi (A) Appl Mater Sci 2021;218:1–17.
[66] Ott NFM, Wills HH. The electrical conductivity of transition metals. Proc R Soc Lond Ser A 1936;153:699–717.
[67] Dai Y, Qi K, Ou K, Song Y, Zhou Y, Zhou M, et al. Ag NW-Embedded coaxial nanofiber-coated yarns with high stretchability and sensitivity for wearable multi-sensing textiles. ACS Appl Mater Interfaces 2023;15:11244–58.
[68] Shi W, Yang X, Lei L, Huang X, Lin J, Liang Q, et al. A high stretchability fiber based on a synergistic three-dimensional conductive network for wide-range strain sensing. Nanoscale Adv 2015;7:517–23.
[69] Kwon C, Seong D, Ha J, Chun D, Bae JH, Yoon K, et al. Self-bondable and stretchable conductive composite fibers with spatially controlled percolated Ag nanoparticle networks: novel integration strategy for wearable electronics. Adv Funct Mater 2020;30:1–10.
[70] Min WK, Won C, Kim DH, Lee S, Chung J, Cho S, et al. Strain-driven negative resistance switching of conductive fibers with adjustable sensitivity for wearable healthcare monitoring systems with near-zero standby power. Adv Mater 2023;35:2303556.
[71] Kim H, Shaqeel A, Han S, Kang J, Yun J, Lee M, et al. In situ formation of Ag nanoparticles for fiber strain sensors: toward textile-based wearable applications. ACS Appl Mater Interfaces 2021;13:39868–79.
[72] Du T, Han X, Yan X, Shang J, Li Y, Song J. MXene-based flexible sensors: materials, preparation, and applications. Adv Mater Technol 2023;8:1–26.

[73] Wu Z, Wei L, Tang S, Xiong Y, Qin X, Luo J, et al. Recent progress in Ti3C2T x MXene-based flexible pressure sensors. ACS Nano 2021;15:18880–94.
[74] Shahzad F, Iqbal A, Kim H, Koo CM. 2D transition metal carbides (MXenes): applications as an electrically conducting material. Adv Mater 2020;32:1–23.
[75] Yu Q, Pan J, Jiang Z, Guo Z, Jiang J. Stretchable multimodal textile sensor based on core-sheath CB/PDMS/MXene sensing yarn for efficiently distinguishing mechanical stimulus. Chem Eng J 2024;493:1–12.
[76] Seyedin S, Uzun S, Levitt A, Anasori B, Dion G, Gogotsi Y, et al. MXene composite and coaxial fibers with high stretchability and conductivity for wearable strain sensing textiles. Adv Funct Mater 2020;30:1–11.
[77] Cao J, Jiang Y, Li X, Yuan X, Zhang J, He Q, et al. A flexible and stretchable MXene/Waterborne polyurethane composite-coated fiber strain sensor for wearable motion and healthcare monitoring. Sensors 2024;24:1–12.
[78] Park YG, Lee GY, Jang J, Yun SM, Kim E, Park JU. Liquid metal-based soft electronics for wearable healthcare. Adv Healthc Mater 2021;10:1–26.
[79] Cademartiri L, Thuo MM, Nijhuis CA, Reus WF, Tricard S, Barber JR, et al. Electrical resistance of Ag TS-S(CH 2) n -1CH 3//Ga 2O 3/EGaIn tunneling junctions. J Phys Chem C 2012;116:10848–60.
[80] Dickey MD, Chiechi RC, Larsen RJ, Weiss EA, Weitz DA, Whitesides GM. Eutectic gallium-indium (EGaIn): a liquid metal alloy for the formation of stable structures in microchannels at room temperature. Adv Funct Mater 2008;18:1097–104.
[81] Víllora EG, Morioka Y, Atou T, Sugawara T, Kikuchi M, Fukuda T. Infrared reflectance and electrical conductivity of β-Ga2O3. Physica Status Solidi A Appl Res 2002;193:187–95.
[82] Zhang Y, Zhang D, Chen Y, Lin H, Zhou X, Zhang Y, et al. Liquid metal enabled elastic conductive fibers for self-powered wearable sensors. Adv Mater Technol 2023;8:1–10.
[83] Li H, Qu R, Ma Z, Zhou N, Huang Q, Zheng Z. Permeable and patternable super-stretchable liquid metal fiber for constructing high-integration-density multifunctional electronic fibers. Adv Funct Mater 2024;34:1–11.
[84] Yang Y, Liu J, Chen G, Gao A, Wang J, Wang J. Stretchable fibers with highly conductive surfaces and robust electromechanical performances for electronic textiles. ACS Appl Mater Interfaces 2024;16:6122–32.
[85] Katouah H, El-Metwaly NM. Plasma treatment toward electrically conductive and superhydrophobic cotton fibers by in situ preparation of polypyrrole and silver nanoparticles. React Funct Polym 2021;159:1–10.
[86] Grancarić AM, Jerković I, Koncar V, Cochrane C, Kelly FM, Soulat D, et al. Conductive polymers for smart textile applications. J Ind Text 2018;48:612–42.
[87] Chen Z, Chen J, Ge H, Gao Q, Zhu J, Zhu C, et al. Unique core-shell organogel/hydrogel fibers with tunable assembly structures for personal thermal management and human motion detection. Eng J 2025;518:164807.
[88] Gao Y, Yu L, Li Y, Wei L, Yin J, Wang F, et al. Maple leaf inspired conductive fiber with hierarchical wrinkles for highly stretchable and integratable electronics. ACS Appl Mater Interfaces 2022;14:49059–71.
[89] Jain K, Wang Z, Garma LD, Engel E, Ciftci GC, Fager C, et al. 3D printable composites of modified cellulose fibers and conductive polymers and their use in wearable electronics. Appl Mater Today 2023;30:1–11.
[90] Mishra K, Devi N, Siwal SS, Zhang Q, Alsanie WF, Scarpa F, et al. Ionic liquid-based polymer nanocomposites for sensors, energy, biomedicine, and environmental applications: roadmap to the future. Adv Sci 2022;9:1–50.
[91] Anceschi A, Riccardi C, Patrucco A. The role of ionic liquids in textile processes: a comprehensive review. Molecules 2025;30:1–23.
[92] Zhao C, Zhang C, Wang P, Chen Z, Wang Y, Zhu J, et al. Wet-spun PEDOT: pss/ionic liquid composite fibers for wearable e-Textiles. Eur Polym J 2023;190:1–8.
[93] Chen H, Xu H, Luo M, Wang W, Qing X, Lu Y, et al. Highly conductive, ultrastrong, and flexible wet-spun PEDOT:PSS/ionic liquid fibers for wearable electronics. ACS Appl Mater Interfaces 2023;15:20346–57.
[94] Wang K, Wang XX, Wang CY, Yin M, Yu SS, Chen KZ, et al. Customizable and scalable manufacture of aesthetic ionic conductive silk yarns for e-textile devices. Chem Eng J 2024;487:1–9.
[95] Wu Y, Wei F, Li T, Li M, Pei D, Li C. Zwitterionic liquid crystal elastomer with unusual dependence of ionic conductivity on strain and temperature for smart wearable fabric. Chem Eng J 2024;489:1–8.
[96] Zhao L, Wang B, Mao Z, Sui X, Feng X. Nonvolatile, stretchable and adhesive ionogel fiber sensor designed for extreme environments. Chem Eng J 2022;433:1–10.
[97] Cao Z, Wang R, He T, Xu F, Sun J. Interface-controlled conductive fibers for wearable strain sensors and stretchable conducting wires. ACS Appl Mater Interfaces 2018;10:14087–96.
[98] Qi X, Wang W, Dai H, Zhu Y, Dong Y, Fu SY, et al. Multifunctional two-way shape memory RGO/ethylene-vinyl acetate composite yarns for electro-driven actuators and high sensitivity strain sensors. Compos - A: Appl Sci Manuf 2023;169:1–11.
[99] Wang J, Huang S, Lu X, Xu Z, Zhao Y, Li J, et al. Wet-spinning of highly conductive nanocellulose–silver fibers. J Mater Chem C 2017;7:9673–9.
[100] Lee J, Lee DM, Jung Y, Park J, Lee HS, Kim YK, et al. Direct spinning and densification method for high-performance carbon nanotube fibers. Nat Commun 2019;10:1–10.
[101] Guo X, Zhang Y, Li J, Hao Y, Ke H, Lv P, et al. Wet spinning technology for aerogel fiber: pioneering the frontier of high-performance and multifunctional materials. Adv Fiber Mater 2024;6:1669–709.
[102] Xu Z, Zhou J, Li D, Zhu G, Lin N. Flexible conductive fibers from alginate, cellulose nanocrystals, and polyaniline by wet spinning. Chem Eng 2023;11:10895–905.
[103] Shi W, Chen S, Lin Y, Zhang G, Peng Z, Liu Z, et al. Piezoresistive fibers with record high sensitivity via the synergic optimization of porous microstructure and elastic modulus. Chem Eng J 2022;441:1–9.
[104] Huang J, Wei Q, Zhao M. Flexible and stretchable Poly(styrene-butadiene-styrene)/MXene nanosheet composite and coaxial fibers for wearable. Strain Sensors ACS Appl Nano Mater 2023;6:8743–51.
[105] Chen S, Jiang S, Qiao D, Wang J, Zhou Q, Wu C, et al. Chinese tofu-inspired biomimetic conductive and transparent fibers for biomedical applications. Small Methods 2023;7:1–9.
[106] Niu B, Yang S, Yang Y, Hua T. Highly conductive fiber with design of dual conductive Ag/CB layers for ultrasensitive and wide-range strain sensing. SmartMat 2023;4:1–14.
[107] Li W, Zhou Y, Wang Y, Li Y, Jiang L, Ma J, et al. Highly stretchable and sensitive SBS/graphene composite fiber for strain sensors. Macromol Mater Eng 2020;305:1–9.
[108] Li C, Wang S, Luo Y, Yu D, Wang L, Wang Y, et al. Ultra-high elongation MXene/Polyurethane porous fibers with passive insulation, passive radiative heating and active heating properties for personal thermal management. Chem Eng J 2024;500:157186.
[109] Morad MR, Rajabi A, Razavi M, Pejman Sereshkeh SR. A very stable high throughput taylor cone-jet in electrohydrodynamics. Sci Rep 2016;6:1–10.
[110] Zhu C, Zheng J, Fu J. Electrospinning nanofibers as stretchable sensors for wearable devices. Macromol Biosci 2024;24:1–16.
[111] Liu Z, Ma J, Zhang P. Fabrication of stretchable and conductive liquid metal microfibers through coaxial emulsion electrospinning. Adv Eng Mater 2025:1–10.
[112] Glauß B, Steinmann W, Walter S, Beckers M, Seide G, Gries T, et al. Spinnability and characteristics of polyvinylidene fluoride (PVDF)-based bicomponent fibers with a carbon nanotube (CNT) modified polypropylene core for piezoelectric applications. Materials 2013;6:2642–61.
[113] Onggar T, Kruppke I, Cherif C. Electric conductive fibers from extrinsic conductive fillers with thermoplastics by melt spinning. Mater Res Express 2024:1–34.
[114] Probst H, Katzer K, Nocke A, Hickmann R, Zimmermann M, Cherif C. Melt spinning of highly stretchable, electrically conductive filament yarns. Polym 2021;13:1–12.
[115] Dejene BK, Abtew MA, Worku BG. Smart core-sheath fibers for advanced textiles: material integration, manufacturing strategies, and applications. Mater Today Adv 2025;28:100655.
[116] Nie M, Li B, Hsieh Y Lo, Fu KK, Zhou J. Stretchable one-dimensional conductors for wearable applications. ACS Nano 2022;16:19810–39.
[117] Wang J, Hu T, Zhou J, Zhao Y, Zhang D, Sheng B. Dip-coated conductive polyurethane fibers composited with liquid metal particles and multiwall carbon nanotubes for multifunctional applications. ACS Appl Nano Mater 2024;8:1–14.
[118] Guo R, Wang H, Chen G, Yuan B, Zhang Y, Liu J. Smart semiliquid metal fibers with designed mechanical properties for room temperature stimulus response and liquid welding. Appl Mater Today 2020;20:1–8.
[119] Liu S, Zhang W, He J, Lu Y, Wu Q, Xing M. Fabrication techniques and sensing mechanisms of textile-based strain sensors: from spatial 1D and 2D perspectives. Adv Fiber Mater 2024;6:36–67.
[120] Liu X, Miao J, Fan Q, Zhang W, Zuo X, Tian M, et al. Smart textile based on 3D stretchable silver Nanowires/MXene conductive networks for personal healthcare and thermal management. ACS Appl Mater Interfaces 2021;13:56607–19.
[121] Tang C, Yang Y, Sun X, Peng H. Scalable production of stretchable conductive fibers for textile electronics. Matter 2023;6:1675–7.
[122] Mukherjee A, Dianatdar A, Gładysz MZ, Hemmatpour H, Hendriksen M, Rudolf P, et al. Electrically conductive and highly stretchable piezoresistive polymer nanocomposites via oxidative chemical vapor deposition. ACS Appl Mater Interfaces 2023;15:31899–916.
[123] Wang K, Sun X, Cheng S, Cheng Y, Huang K, Liu R, et al. Multispecies-coadsorption-induced rapid preparation of graphene glass fiber fabric and applications in flexible pressure sensor. Nat Commun 2024;15:1–10.
[124] Korzeniewska E, De Mey G, Pawlak R, Stempień Z. Analysis of resistance to bending of metal electroconductive layers deposited on textile composite substrates in PVD process. Sci Rep 2020;10:1–11.
[125] Miśkiewicz P, Frydrych I, Cichocka A. Application of physical vapor deposition in textile industry. Autex Res J 2022;22:42–54.
[126] Li Q, Ding C, Yuan W, Xie R, Zhou X, Zhao Y, et al. Highly stretchable and permeable conductors based on shrinkable electrospun fiber mats. Adv Fiber Mater 2021;3:302–11.
[127] Kim D hye, Shin S, Jeon S jae, Han S. High-performance Bismuth–Antimony–Telluride/PEDOT:PSS hybrid thermoelectric fiber prepared by Co-Sputtering. J Alloys Compd 2025;1010:1–9.
[128] Ma Z, Huang Q, Zhou N, Zhuang Q, Ng SW, Zheng Z. Stretchable and conductive fibers fabricated by a continuous method for wearable devices. Cell Rep Phys Sci 2023;4.
[129] Stuart S, de Kok M, O'Searcoid B, Morrisroe H, Serban IB, Jagers F, et al. Critical design considerations for longer-term wear and comfort of On-Body medical devices. Bioeng 2024;11:1–20.
[130] Hasan MM, Hossain MM. Nanomaterials-patterned flexible electrodes for wearable health monitoring: a review. J Mater Sci 2021;56:14900–42.
[131] Stern S. Electrocardiogram: still the cardiologist's best friend. Circ 2006;113:753–6.
[132] Pani D, Achilli A, Bonfiglio A. Survey on textile electrode technologies for electrocardiographic (ECG) monitoring, from metal wires to polymers. Adv Mater Technol 2018;3:1–14.
[133] Yan X, Chen S, Zhang G, Shi W, Peng Z, Liu Z, et al. Highly breathable, surface-hydrophobic and wet-adhesive silk based epidermal electrode for long-term electrophysiological monitoring. Compos Sci Technol 2022;230:109751.

[134] Cao P, Wang Y, Yang J, Niu S, Pan X, Lu W, et al. Scalable layered heterogeneous hydrogel fibers with strain-induced crystallization for tough, resilient, and highly conductive soft bioelectronics. Adv Mater 2024;36:1–12.
[135] Hu S, Song J, Tian Q, Zeng C, Jiang Y, Li Q, et al. Mechanically and conductively robust eutectogel fiber produced by continuous wet spinning enables epidermal and implantable electrophysiological monitoring. Adv Fiber Mater 2024;6:1980–91.
[136] Kim SH, Kim Y, Choi H, Park J, Song JH, Baac HW, et al. Mechanically and electrically durable, stretchable electronic textiles for robust wearable electronics. RSC Adv 2021;11:22327–33.
[137] Dong J, Tang X, Peng Y, Fan C, Li L, Zhang C, et al. Highly permeable and ultrastretchable E-textiles with EGaIn-superlyophilicity for on-skin health monitoring, joule heating, and electromagnetic shielding. Nano Energy 2023;108.
[138] Motiepor K, Bakhtiyari S, Jahanshahi A, Bagherzadeh R. Stretchable clutter-free E-Textile EEG cap: advancing seamless wearable solutions for emerging neuroimaging applications. Sens Actuators A Phys 2025;387:1–10.
[139] Xu K, Lu Y, Takei K. Multifunctional skin-inspired flexible sensor systems for wearable electronics. Adv Mater Technol 2019;4:1–25.
[140] Fakharuddin A, Li H, Di Giacomo F, Zhang T, Gasparini N, Elezzabi AY, et al. Fiber-shaped electronic devices. Adv Energy Mater 2021;11:1–58.
[141] Liu H, Li Q, Zhang S, Yin R, Liu X, He Y, et al. Electrically conductive polymer composites for smart flexible Strain sensors: a critical review. J Mater Chem C 2018;6:12121–41.
[142] Wang X, Zhao X, Yu Y, Zhai W, Yue X, Dai K, et al. Design of flexible micro-porous fiber with double conductive network synergy for high-performance strain sensor. Chem Eng J 2024;495:1–9.
[143] Han K, Kim I, Lee E, Bae GY, Yang C. Liquid metal composite-based flexible pressure sensors with high sensitivity. ACS Appl Mater Interfaces 2025;17:40994–1001.
[144] Y Huang Y, Fan X, Chen SC, Zhao N. Emerging technologies of flexible pressure sensors: materials, modeling, devices, and manufacturing. Adv Funct Mater 2019;29:1–24.
[145] Zhang J wen, Zhang Y, yuan Li Y, Wang P. Textile-based flexible pressure sensors: a review. Polym Rev 2022:65–94.
[146] Zhi C, Shi S, Si Y, Fei B, Huang H, Hu J. Recent progress of wearable piezoelectric pressure sensors based on nanofibers, yarns, and their fabrics via electrospinning. Adv Mater Technol 2023;8:1–33.
[147] Tang J, Zou Y, Liu C, Lv Y. Liquid metal fiber-based high-sensitivity strain and pressure sensors enhanced by porous structure. ACS Appl Electron Mater 2024;6:7512–21.
[148] Arman Kuzubasoglu B, Kursun Bahadir S. Flexible temperature sensors: a review. Sens Actuators A: Phys 2020;315:1–16.
[149] Soomro AM, Jawed B, Qayoom A, Hyder H, Hussain K, Iram L, et al. Textile-based flexible temperature sensors for wearable and sports applications. Phys Status Solidi (A) Appl Mater Sci 2024;221:1–29.
[150] Cai J, Du M, Li Z. Flexible temperature sensors constructed with fiber materials. Adv Mater Technol 2022;7:1–16.
[151] Ban J, Lu Y, Lu J, Jia K, Luo M, Zhou Y, et al. Highly sensitive stretchable fiber-based temperature sensor enhanced by surface-chemically modified silver nanowires. Chem Eng J 2024;482:1–8.
[152] Rauf S, Vijjapu MT, Andrés MA, Gascón I, Roubeau O, Eddaoudi M, et al. Highly selective metal–organic framework textile humidity sensor. ACS Appl Mater 2020;580:29999–30006.
[153] Li J, Fang Z, Wei D, Liu Y. Flexible pressure, humidity, and temperature sensors for human health monitoring. Adv Healthc Mater 2024;13:1–37.
[154] Yan S, Shen D, Newton MAA, Zhu S, Xin B. Patterned, flexible, self-supporting humidity sensor with core-sheath structure for real-time sensing of human-related humidity. Colloids Surf, A Physicochem Eng Asp 2024;695.
[155] Faruk MO, Ahmed A, Jalil MA, Islam MT, Shamim AM, Adak B, et al. Functional textiles and composite based wearable thermal devices for joule heating: progress and perspectives. Appl Mater Today 2021;23:1–23.
[156] Ye C, Zhao L, Yang S, Li X. Recent research on preparation and application of smart joule heating fabrics. Small 2024;20:1–32.
[157] Yu X, Fan W, Liu Y, Dong K, Wang S, Chen W, et al. A one-step fabricated sheath-core stretchable fiber based on liquid metal with superior electric conductivity for wearable sensors and heaters. Adv Mater Technol 2022;7:1–8.
[158] Yi P, Zou H, Yu Y, Li X, Li Z, Deng G, et al. MXene-Reinforced liquid metal/polymer fibers via interface engineering for wearable multifunctional textiles. ACS Nano 2022;16:14490–502.
[159] Koo JH, Kim DC, Shim HJ, Kim TH, Kim DH. Flexible and stretchable smart display: materials, fabrication, device design, and system integration. Adv Funct Mater 2018;28:1–23.
[160] Heo JS, Eom J, Kim YH, Park SK. Recent progress of textile-based wearable electronics: a comprehensive review of materials, devices, and applications. Small 2018;14:1–16.
[161] Kim H, Kwon YT, Lim HR, Kim JH, Kim YS, Yeo WH. Recent advances in wearable sensors and integrated functional devices for virtual and augmented reality applications. Small 2018;14:1–16.
[162] Hwang YH, Kong SU, Kim CY, Lee J, Cho HE, Jeong SY, et al. Organic light-emitting fibers and fabrics for truly wearable smart displays: recent progress and future opportunities. J Soc Inf Disp 2022;30:727–47.
[163] Hwang YH, Kwon S, Shin J Bin, Kim H, Son YH, Lee HS, et al. Bright-multicolor, highly efficient, and addressable phosphorescent organic light-emitting fibers: toward wearable textile information displays. Adv Funct Mater 2021;31:1–10.
[164] Wang H, Yue X, Shen X, Wang X, Zheng R, Han Q, et al. Fabrication of pressure visual fiber based on liquid metal control thermochromic pigments. Polym Compos 2024;45:12636–48.
[165] Shi X, Zuo Y, Zhai P, Shen J, Yang Y, Gao Z, et al. Large-area display textiles integrated with functional systems. Nat 2021;591:240–5.
[166] Dolez PI. Energy harvesting materials and structures for smart textile applications: recent progress and path forward. Sensors 2021;21:1–27.
[167] Komolafe A, Zaghari B, Torah R, Weddell AS, Khanbareh H, Tsikriteas ZM, et al. E-textile technology review–from materials to application. IEEE Access 2021;9:97152–79.
[168] Huang L, Lin S, Xu Z, Zhou H, Duan J, Hu B, et al. Fiber-based energy conversion devices for human-body energy harvesting. Adv Mater 2020;32:1–20.
[169] Tao X. Study of fiber-based wearable energy systems. Acc Chem Res 2019;52:307–15.
[170] Zeng W, Shu L, Li Q, Chen S, Wang F, Tao XM. Fiber-based wearable electronics: a review of materials, fabrication, devices, and applications. Adv Mater 2014;26:5310–36.
[171] Wu Y, Dai X, Sun Z, Zhu S, Xiong L, Liang Q, et al. Highly integrated, scalable manufacturing and stretchable conductive core/shell fibers for strain sensing and self-powered smart textiles. Nano Energy 2022;98:1–10.
[172] Veeramuthu L, Cho CJ, Venkatesan M, Kumar GR, Hsu HY, Zhuo BX, et al. Muscle fibers inspired electrospun nanostructures reinforced conductive fibers for smart wearable optoelectronics and energy generators. Nano Energy 2022;101:1–11.
[173] Chung KY, Xu B, Li Z, Liu Y, Han J. Bioinspired ultra-stretchable dual-carbon conductive functional polymer fiber materials for health monitoring, energy harvesting and self-powered sensing. Chem Eng J 2023;454:1–12.
[174] Qi K, Zhou Y, Ou K, Dai Y, You X, Wang H, et al. Weavable and stretchable piezoresistive carbon nanotubes-embedded nanofiber sensing yarns for highly sensitive and multimodal wearable textile sensor. Carbon 2020;170:464–76.
[175] Tang Z, Jia S, Wang F, Bian C, Chen Y, Wang Y, et al. Highly stretchable core–sheath fibers via wet-spinning for wearable strain sensors. ACS Appl Mater Interfaces 2018;10:6624–35.
[176] Wang X, Liu X, Schubert DW. Highly sensitive ultrathin flexible thermoplastic polyurethane/carbon Black fibrous film strain sensor with adjustable scaffold networks. Nano-Micro Lett 2021;13:1–19.
[177] Shen J, Li C, Hou S, Li C, Yin K, Bi H, et al. Continuous preparation of highly robust TPU/CNT conductive aerogel fibers with heterogeneous hierarchical structure for multifunctional applications. Chem Eng J 2025;506:1–11.
[178] Wang X, Sun H, Yue X, Yu Y, Zheng G, Dai K, et al. A highly stretchable carbon nanotubes/thermoplastic polyurethane fiber-shaped strain sensor with porous structure for human motion monitoring. Compos Sci Technol 2018;168:126–32.
[179] Sun Y, Wang Y, Hua C, Ge Y, Hou S, Shang Y, et al. Water-responsive helical graphene-oxide fibers incorporating a continuous carbon nanotube network. Carbon 2018;132:394–400.
[180] Zhang P, Guo C, Huang L, Li Y, Zhang K, Zhang Y. Highly stretchable serpentine-shaped strain sensor based on 3D printing for gestures recognition. IEEE Trans Instrum Meas 2024;73.
[181] Wang J, Liu B, Li D, Yuan J, Huang D, Zhang C, et al. Fiber-shaped, stretchable strain sensors with high linearity by one-step injection molding for structural health monitoring. Adv Funct Mater 2025;35:2500701.
[182] Sun F, Tian M, Sun X, Xu T, Liu X, Zhu S, et al. Stretchable conductive fibers of ultrahigh tensile strain and stable conductance enabled by a worm-shaped graphene microlayer. Nano Lett 2019;19:6592–9.
[183] Won C, Lee S, Jung HH, Woo J, Yoon K, Lee J, et al. Ultrasensitive and stretchable conductive fibers using percolated Pd nanoparticle networks for multisensing wearable electronics: crack-based strain and H2 sensors. ACS Appl Mater Interfaces 2020;12:45243–53.
[184] Zhang W, Miao J, Tian M, Zhang X, Fan T, Qu L. Hierarchically interlocked helical conductive yarn enables ultra-stretchable electronics and smart fabrics. Chem Eng J 2023;462:1–12.
[185] Li J, Wang L, Wang X, Yang Y, Hu Z, Liu L, et al. Highly conductive PVA/Ag coating by aqueous in situ reduction and its stretchable structure for strain sensor. ACS Appl Mater Interfaces 2019;12:1427–35.
[186] Pan W, Wang J, Li YP, Sun XB, Wang JP, Wang XX, et al. Facile preparation of highly stretchable TPU/Ag nanowire strain sensor with spring-like configuration. Polymers 2020;12:1–15.
[187] Koshi T, Nomura KI, Yoshida M. Measurement and analysis on failure lifetime of serpentine interconnects for e-textiles under cyclic large deformation. Flex Print Electron 2021;6:1–11.
[188] Li P, Zhang W, Ma J, Wang X, Xu H, Cong L, et al. Solution-grown serpentine silver nanofiber meshes for stretchable transparent conductors. Adv Electron Mater 2018;4:1–7.
[189] Wang R, Zhai Q, An T, Gong S, Cheng W. Stretchable gold fiber-based wearable textile electrochemical biosensor for lactate monitoring in sweat. Talanta 2021;222:1–8.
[190] Wei Y, Chen S, Yuan X, Wang P, Liu L. Multiscale wrinkled microstructures for piezoresistive fibers. Adv Funct Mater 2016;26:5078–85.
[191] Chen T, Wei P, Chen G, Liu H, Mugaanire IT, Hou K, et al. Heterogeneous structured tough conductive gel fibres for stable and high-performance wearable strain sensors. J Mater Chem A 2021;9:12265–75.
[192] Ding Y, Xu W, Wang W, Fong H, Zhu Z. Scalable and facile preparation of highly stretchable electrospun PEDOT: PSS@ PU fibrous nonwovens toward wearable conductive textile applications. ACS Appl Mater Interfaces 2017;9:30014–23.
[193] Wu Y, Yan T, Zhang K, Pan Z. A hollow core-sheath composite fiber based on polyaniline/polyurethane: Preparation, properties, and multi-model strain sensing performance. Adv Mater Technol 2023;8:2200777.

[194] Wang M, Gao Q, Gao J, Zhu C, Chen K. Core-shell PEDOT:PSS/SA composite fibers fabricated: via a single-nozzle technique enable wearable sensor applications. J Mater Chem C 2020;8:4564–71.
[195] Chen J, Zhu J, Wei Z, Chen Z, Zhu C, Gao Q, et al. Highly stretchable and elastic PEDOT: PSS helix fibers enabled wearable sensors. J Mater Chem C 2023;11: 13358–69.
[196] Sun T, Liang Y, Ning N, Wu H, Tian M. Strain-insensitive stretchable conductive fiber based on helical core with double-network hydrogel. Adv Fiber Mater 2025; 7:882–93.
[197] Chen S, Li J, Liu H, Shi W, Peng Z, Liu L. Pruney fingers-inspired highly stretchable and sensitive piezoresistive fibers with isotropic wrinkles and robust interfaces. Chem Eng J 2022;430:1–10.
[198] Chen G, Wang H, Guo R, Duan M, Zhang Y, Liu J. Superelastic EGaIn composite fibers sustaining 500% tensile strain with superior electrical conductivity for wearable electronics. ACS Appl Mater Interfaces 2020;12:6112–8.
[199] Zhou J, Zhao S, Tang L, Zhang D, Sheng B. Programmable and weldable superelastic EGaIn/TPU composite fiber by wet spinning for flexible electronics. ACS Appl Mater Interfaces 2023;15:1–12.
[200] Zhang Y, He Y, Niu L, Xing X, Jiang Y, Fang J, et al. Enhanced sensing performance of superelastic thermally drawn liquid metal fibers through helical architecture while eliminating directional signal errors. J Mater Sci Technol 2024; 195:136–45.
[201] Luo M, Wei W, Guo Q, Zhong W, Jia K, Chang K, et al. A liquid metal-embedded sheath-core fiber with internal helical structure for strain-insensitive electronics. Adv Sci 2025:e09547.
[202] Fu C, Tang W, Miao Y, Xu A, Nilghaz A, Xu W, et al. Large-scalable fabrication of liquid metal-based double helix core-spun yarns for capacitive sensing, energy harvesting, and thermal management. Nano Energy 2023;106:1–13.
[203] Tang J, Chen S, Wen Z, Zhang Z, Sheng B, Wang J. Bio-inspired helical EGaIn/ TPU conductive fibers fabricated by a twisted coating method for flexible electronics. J Mater Chem C 2025;13:3341–51.
[204] Zhou N, Jiang B, He X, Li Y, Ma Z, Zhang H, et al. A superstretchable and ultrastable liquid metal–elastomer wire for soft electronic devices. ACS Appl Mater Interfaces 2021;13:19254–62.
[205] Li Q, Li K, Fan H, Hou C, Li Y, Zhang Q, et al. Reduced graphene oxide functionalized stretchable and multicolor electrothermal chromatic fibers. J Mater Chem C 2017;5:11448–53.
[206] Wang Y, Niu W, Lo CY, Zhao Y, He X, Zhang G, et al. Interactively full-color changeable electronic fiber sensor with high stretchability and rapid response. Adv Funct Mater 2020;30:2000356.
[207] He R, Zhao B, Gu C, Yin S, Wang Y, Qin W. Core-Shell porous LM/TPU fibers with tunable conductive properties for use as strain and pressure sensors. Compos Commun 2024;51:102075.
[208] Wu Y, Wang F, Wang Z, Liu S, Yu J, Ding B, et al. Highly stretchable, resistance-stable, conductive liquid metal core-sheath fibers enable ultrastable and supersensitive physiological monitoring. Small 2025:e0739.
[209] Zhuang J, Liu Y, Bian D, He F, Li Y, Fan W. Spinning solution viscosity reducing and wet spinning of carbon black-based elastic conductive fibers for sports monitoring and healthcare electrical heating. J Mater Res Technol-JMRT 2025; 36:1–12.
[210] Han X, Xiao W, Wen S, Lin J, He A, Jiang Q, et al. High-performance stretchable strain sensor based on Ag nanoparticles sandwiched between two 3D-Printed polyurethane fibrous textiles. Adv Electron Mater 2021;7:2001242.
[211] Wang R, Xie L, Zhang Z, Sun H, Xiao Y. Mussel-inspired wet-spun conductive fibers for stretchable electronics. Compos Commun 2025;53:102171.
[212] Lu H, Zhang Y, Zhu M, Li S, Liang H, Bi P, et al. Intelligent perceptual textiles based on ionic-conductive and strong silk fibers. Nat Commun 2024;15:1–9.
[213] Xu Y, Feng Q, Zhang C, Liu T. Wet-spinning of ionic liquid@elastomer coaxial fibers with high stretchability and wide temperature resistance for strain sensors. Compos Commun 2021;25:1–6.
[214] Ye H, Wu B, Sun S, Wu P. A solid–liquid bicontinuous fiber with strain-insensitive ionic conduction. Adv Mater 2024;36:1–10.
[215] Wang XP, Guo JR, Hu L. Preparation and application of gallium-based conductive materials in the very recent years. Sci China Technol Sci 2021;64:681–95.
[216] Chen S, Wang HZ, Zhao RQ, Rao W, Liu J. Liquid metal composites. Matter 2020; 2:1446–80.
[217] Schneider R, Facure MHM, Chagas PAM, Andre RS, dos Santos DM, Correa DS. Tailoring the surface properties of micro/nanofibers using 0D, 1D, 2D, and 3D nanostructures: a review on post-modification methods. Adv Mater Interfaces 2021;8:1–28.
[218] Lv Y, Min L, Niu F, Qin Z, Zhang M, Zhao B, et al. Conductive nanomaterials with different dimensions for flexible piezoresistive sensors: from selectivity to applications. Adv Mater Technol 2023;8:1–15.
[219] Kang L, Ma J, Wang C, Li K, Wu H, Zhu M. Highly sensitive and wide detection range thermoplastic polyurethane/graphene nanoplatelets multifunctional strain sensor with a porous and crimped network structure. ACS Appl Mater Interfaces 2024;16:2814–24.
[220] Ruiz-Calleja T, Jiménez-Suárez A, Sainz-de-Robles F, Cristóbal-Ruiz P. Effect of calendering on the performance of 100% recycled polyester weft-knitted fabrics. J Ind Textil 2024;54:1–15.
[221] Hwang I, Park HM, Chang YJ. Hinges-in-Foldable-and-Rollable-Devices-Technical-Review n.d. IMID 2021 symposium digest. 2021. p. 333–6.
[222] Lee HJ, Na SC, Lim TG, Yun J, Megra YT, Oh JH, et al. Vertical graphene-decorated carbon nanofibers establishing robust conductive networks for fiber-based stretchable strain sensors. J Mater Sci Technol 2024;200:52–60.
[223] Yang S, Yang W, Yin R, Liu H, Sun H, Pan C, et al. Waterproof conductive fiber with microcracked synergistic conductive layer for high-performance tunable wearable strain sensor. Chem Eng J 2023;453:1–9.
[224] Ren M, Li J, Zhao Y, Zhai W, Zhou K, Yu Y, et al. Highly strain-sensitive and stretchable multilayer conductive composite based on aligned thermoplastic polyurethane fibrous mat for human motion monitoring. Compos Commun 2024; 46:1–8.
[225] Niu B, Yang S, Tian X, Hua T. Highly sensitive and stretchable fiber strain sensors empowered by synergetic conductive network of silver nanoparticles and carbon nanotubes. Appl Mater Today 2021;25:1–10.
[226] Wu H, Wang L, Lou H, Wan J, Pu X. One-step coaxial spinning of core-sheath hydrogel fibers for stretchable ionic strain sensors. Chem Eng J 2023;458:1–10.
[227] Liu J, Wang P, Li G, Yang L, Yu W, Meng C, et al. A highly stretchable and ultra-sensitive strain sensing fiber based on a porous core–network sheath configuration for wearable human motion detection. Nanoscale 2022;14: 12418–30.
[228] Gao Q, Wang Y, Wang P, Shen M, Li T, Gao C, et al. Highly stretchable, conductive and long-term stable PEDOT:PSS fibers with surface arrays for wearable sensors. Adv Eng Mater 2022;24:1–9.
[229] Xu S, Yan Y, Zhao Y, Qiu X, Zhuang D, Liu H, et al. Spinnable adhesive functional-hydrogel fibers for sensing and perception applications. J Mater Chem C 2021;9: 5554–64.
[230] Wang W, Yao D, Wang H, Ding Q, Luo Y, Ding H, et al. A breathable, stretchable, and self-calibrated multimodal electronic skin based on hydrogel microstructures for wireless wearables. Adv Funct Mater 2024;34:1–15.
[231] Li L, Zheng Y, Liu E, Zhao X, Yu S, Wang J, et al. Stretchable and ultrasensitive strain sensor based on a bilayer wrinkle-microcracking mechanism. Chem Eng J 2022;437:1–13.
[232] Wang X, Wang X, Pi M, Ran R. High-strength, highly conductive and woven organic hydrogel fibers for flexible electronics. Chem Eng J 2022;428:1–10.
[233] Tian Y, Huang M, Wang Y, Zheng Y, Yin R, Liu H, et al. Ultra-stretchable, sensitive and breathable electronic skin based on TPU electrospinning fibrous membrane with microcrack structure for human motion monitoring and self-powered application. Chem Eng J 2024;480:1–12.
[234] Yue X, Fang C, Yao Q, Liu C, Shen C, Liu H. Tunable porous fiber-shaped strain sensor with synergistic conductive network for human motion recognition and tactile sensing. Chem Eng J 2024;491:1–11.
[235] Wang J, Liu S, Chen Z, Shen T, Wang Y, Yin R, et al. Ultrasensitive electrospinning fibrous strain sensor with synergistic conductive network for human motion monitoring and human-computer interaction. J Mater Sci Technol 2025;213: 213–22.
[236] Wang C, Liu Y, Qu X, Shi B, Zheng Q, Lin X, et al. Ultra-stretchable and fast self-healing ionic hydrogel in cryogenic environments for artificial nerve fiber. Adv Mater 2022;34:1–11.
[237] Zhu L, Zhou X, Zhang J, Xia Y, Wu M, Zhang Y, et al. Self-adhesive elastic conductive ink with high permeability and low diffusivity for direct printing of universal textile electronics. ACS Nano 2024;18:34750–62.
[238] Gao Q, Chen Z, Liu C, Wang Y, Zhu J, Gao C. Helical TPU/Ag@K2Ti4O9 fibers with shape memory performance for highly stretchable and sensitive strain sensors. J Alloys Compd 2024;980:1–11.
[239] Gong J, Tang W, Xia L, Fu Z, Zhou S, Zhang J, et al. Flexible and weavable 3D porous graphene/pPy/Lignocellulose-Based versatile fibrous wearables for thermal management and strain sensing. Chem Eng J 2023;452:1–11.
[240] Miao Z, Yu R, Bai X, Du X, Yang Z, Zhou T, et al. Versatile graphene/ polyelectrolyte aqueous dispersion for fiber-based wearable sensors and electroluminescent devices. China Mater 2024;67:1915–25.
[241] Rotzler S, Schneider-Ramelow M. Washability of E-Textiles: failure modes and influences on washing reliabilit. Textiles 2021;1:37–54.
[242] Rotzler S, Krshiwoblozki M von, Schneider-Ramelow M. Washability of e-textiles: current testing practices and the need for standardization. Textil Res J 2021;91: 2401–17.
[243] Azani MR, Hassanpour A. Electronic textiles (E-Textiles): types, fabrication methods, and recent strategies to overcome durability challenges (washability & flexibility). J Mater Sci Mater Electron 2024;35:1–51.
[244] Wang C, Yokota T, Someya T. Natural biopolymer-based biocompatible conductors for stretchable bioelectronics. Chem Rev 2021;121:2109–46.
[245] Liu G, Lv Z, Batool S, Li MZ, Zhao P, Guo L, et al. Biocompatible material-based flexible biosensors: from materials design to wearable/implantable devices and integrated sensing systems. Small 2023;19:1–43.
[246] Moon S, Chae Y. Colorful graphene-based wearable e-textiles prepared by co-dyeing cotton fabrics with natural dyes and reduced graphene oxide. Sci Rep 2024;14:1–13.
[247] Dang T, Zhao M. The application of smart fibers and smart textiles. J Phys Conf Ser 2021;1790:1–7.
[248] Ryan JD, Mengistie DA, Gabrielsson R, Lund A, Müller C. Machine-washable PEDOT:PSS dyed silk yarns for electronic textiles. ACS Appl Mater Interfaces 2017;9:9045–50.
[249] Zeng Z, Hao B, Li D, Cheng D, Cai G, Wang X. Large-scale production of weavable, dyeable and durable spandex/CNT/cotton core-sheath yarn for wearable strain sensors. Compos. - a. Appl Sci Manuf 2021;149:1–9.

Kangto Han received his B.S. degree in Materials Design Engineering from Kumoh National Institute of Technology (KIT), Republic of Korea, in 2024. He is currently pursuing an M.S. degree in the same department at KIT. His research interests include fiber-based flexible sensors and soft electronic systems.

Eunho Lee is an Associate Professor in the Department of Chemical and Biomolecular Engineering at Seoul National University of Science and Technology (SeoulTech), Republic of Korea. He received his Ph.D. degree in Chemical Engineering from Pohang University of Science and Technology (POSTECH) in 2018. He subsequently worked as a postdoctoral researcher at the Rowland Institute at Harvard University and the University of North Texas. His research focuses on organic mixed-conducting polymers, neuromorphic organic electrochemical transistors, and bio-integrated soft electronic systems.

Jinsu Yun is currently an undergraduate student in the Department of Materials Design Engineering at Kumoh National Institute of Technology (KIT). His research focuses on flexible and deformable electronics fabricated via advanced 3D printing technologies.

Gyojic Shin is a Principal Researcher at the Korea Institute of Industrial Technology (KITECH), Republic of Korea. He obtained his Ph.D. degree in Materials Science and Engineering from Pohang University of Science and Technology (POSTECH) in 2007. His research interests include nanomaterials and their applications in advanced electronic technologies.

Chanmin Lee is a Senior Researcher at the Korea Institute of Industrial Technology (KITECH), Republic of Korea. He earned his Ph.D. degree in Molecular and Material Sciences from Kyushu University, Japan. His current research focuses on inorganic and organic fibrous materials and their applications in catalysis and sensor technologies.

Siyoung Lee is a Senior Researcher in the Advanced Bio and Healthcare Materials Research Division at the Korea Institute of Materials Science (KIMS). He received his B.S. and Ph.D. degrees in Chemical Engineering from Pohang University of Science and Technology (POSTECH) in 2014 and 2020, respectively. Before joining KIMS, he conducted postdoctoral research at POSTECH, the University of Toronto, and the University of Pennsylvania. His research focuses on deformable devices fabricated through microelectromechanical systems (MEMS) for bioapplications.

Geun Yeol Bae is an Assistant Professor in the Department of Materials Design Engineering at Kumoh National Institute of Technology (KIT), Republic of Korea. He received his Ph.D. degree in Chemical Engineering from Pohang University of Science and Technology (POSTECH) in 2018 and subsequently worked as a Researcher at the Korea Institute of Industrial Technology (KITECH) from 2019 to 2021. Over the past decade, his research has focused on developing nanocomposite-based flexible and stretchable electronic devices, including stretchable electrodes, deformable sensors capable of detecting multiple stimuli, and skin-attachable actuators for next-generation smart systems such as health monitoring and electronic skin (E-skin).